1-1-2018

Characterization of Early Acute Inflammation in a Mouse Calvarial Critical-Sized Defect: Augmentation via rhBMP-2 and pGlcNAc Administration

Zachary James Grey
Medical University of South Carolina

Characterization of Early Acute Inflammation in a Mouse Calvarial Critical-Sized Defect: Augmentation via rhBMP-2 and pGlcNAc Administration

By
Zachary James Grey

A thesis submitted to the faculty of the Medical University of South Carolina in partial fulfillment of the requirements for the degree of Master of Science in the College of Graduate Studies.

Department of Oral Health Sciences
Department of Regenerative Medicine

2018

Approved by:

`

James J. Cray
Chairman, Advisory Committee

Carl Atkinson
Member, Advisory Committee

Jeffrey A. Jones
Member, Advisory Committee

Amanda C. LaRue
Member, Advisory Committee

Robin C. Muise-Helmerick
Member, Advisory Committee

ACKNOWLEDGEMENTS

The completion of this thesis would not have been possible without the steadfast support of the many individuals who have taken their time to invest in my education and training. First, I would like to thank my mentor, Dr. James Cray, for welcoming me into his lab and taking me on as a student. I would also like to thank my lab mates, Dr. R. Nicole Howie and Emily Durham, for their instruction and patience during my training. Further, I am very appreciative of the students who have rotated through our lab, SarahRose Hall, Nick Larson, Brayden Oaks, and Reed Houck, for help in acquiring and interpreting data. Thank you to Dr. Russell Norris for his assistance on my thesis proposal and Dr. Laura Kasman for her guidance throughout this part of my education. I would also like to thank Dr. Paula Traktman for her assistance in navigating towards this degree. Finally, I would like to give a very special thank you to my friends and family for their ongoing support through this entire process.

ABSTRACT

ZACHARY JAMES GREY. Characterization of Early Acute Inflammation in a Mouse Calvarial Critical-Sized Defect: Augmentation via rhBMP-2 and pGlcNAc Administration. (Under the direction of JAMES J. CRAY)

Background

Currently, the gold standard intervention for substantially large bone wounds is autologous bone grafting. While effective, this therapy is complicated by creation of an invasive second surgical site and limited material available for harvest. INFUSE® Bone Graft (rhBMP-2 delivered via an absorbable collagen sponge or ACS) has been widely used as a graft substitute, resulting in robust bone formation, but at the cost of increased inflammation and often poor healing outcomes. A better understanding of the mechanisms by which rhBMP-2 influences inflammatory processes and how these processes can be modulated through other therapies will inform future novel pharmacological avenues to improve patient outcomes.

Hypothesis

Delivery of rhBMP-2 will result in increased inflammation (prolonged M1 response, delayed M2 response) and increased angiogenesis. Administration of pGlcNAc nanofibers will result in a reduced inflammation.

Methods

Calvarial defects (5mm) were created in wild-type mice. Defects were treated with ACS alone (control), ACS loaded with rhBMP-2, or a pGlcNAc nanofiber scaffold. Mice were sacrificed at 3 and 7 days post-operation and calvariae were isolated for downstream analyses. Isolated protein was subjected to western blotting. Mounted tissue sections were stained with hematoxylin and eosin for morphological characterization within the defect. Further, immunohistochemistry for

markers of inflammation and macrophage polarization were performed and analyzed for effects on inflammation and tissue repair.

Results

Baseline characterization of ACS alone indicated little change in markers associated with inflammation from three to seven days. Additionally, delivery of rhBMP-2 led to a delay in macrophage response, but had little effect on macrophage polarization. Angiogenesis was down early in response to rhBMP-2, but resolved to normal levels by day seven. The addition of pGlcNAc to the calvarial defect did not dampen inflammation compared to the baseline control. Further, this treatment had little effect on angiogenesis compared to the ACS alone.

Conclusions

This subclinical dose of rhBMP-2 did not lead to further or sustained inflammation compared to the baseline control. Further, the addition of pGlcNAc did not result in a localized down regulation of inflammation. Identifying other methods for delivery of rhBMP-2 and alternative dosing schemas may prove beneficial in improving patient outcome.

TABLE OF CONTENTS

LIST OF FIGURES

LIST OF TABLES

CHAPTER 1

Statement of Problem

Bone is unique in that it not only provides structure for the body, but also functions in hematopoiesis, storage of essential minerals, and protection of internal organs. Highly dynamic and vascularized, bone undergoes constant remodeling in response to various mechanical stresses.[1-3] Upon damage, bone possesses the innate capacity for regeneration, though complete union of the regenerate is highly dependent on proximity of the surgical margins, following a procedure, or fracture edges following trauma.[2] Furthermore, spontaneous regeneration of bone may be impaired if the individual is under certain metabolic restriction or has an impaired health status (i.e. immunosuppression, age, etc.). As such, injury resulting in large portions of ablated or disarticulated bones poses a serious problem for medicine. Many attempts to alleviate these "non-unions" have been employed and are under continuous investigation. The current "gold standard" for patients with substantial bone injury is autologous bone grafting with tissue harvested from several areas including the iliac crest, mandibular symphysis, or the mandibular ramus.[4-6] While effective, limited supply of donor site grafts and associated harvest site co-morbidity have necessitated the search for alternative means of increasing bone repair efficiency.[5,7,8]

Several therapeutics have emerged in response to this dilemma including adjunctive cell therapy, implantation of biomaterials and scaffolds, and manipulations of osteogenic signaling pathways.[9-11] Of note, INFUSE® Bone Graft (Medtronic, Inc.) has proven effective in therapeutic bone healing and is currently FDA approved for four clinical indications; spinal fusions, tibial shaft fractures, and oral-maxillofacial procedures (sinus lift and ridge augmentation). INFUSE® is a combination therapy, delivering osteoinductive recombinant human *bone morphogenetic protein 2* (rhBMP-2) to the wound site via an osteoconductive scaffold (*absorbable collagen sponge*, ACS). The use of INFUSE® has stretched far beyond its clinical indications and now, nearly 90% of its use is off-label, such as in pediatric (cleft palate surgery) and iatrogenic

procedures (bone neoplasia). Recently, the widespread use of INFUSE® has come into question due to several negative clinical side effects including ectopic bone formation, osteolysis, urogenital problems, and complications as a result of heightened and persistent inflammation.[12,13]

Tight regulation of inflammation following injury is critically important for proper healing in all tissues. Although acute inflammation is absolutely necessary for proper bone healing, dysregulation of this cascade can result in chronic inflammatory diseases and further tissue damage.[1,2,14] Persistent up-regulation of pro-inflammatory stimuli following administration of INFUSE® is a potential mechanism leading to therapeutic failure and, thus, is a promising target for investigation.[12] Systemic down-regulation of inflammation through NSAIDS or corticosteroids can certainly counteract this effect, but results in the alteration of normal inflammation in response to injury and infection. Furthermore, the use of corticosteroids has been associated with a reduction in osteoblast activity and matrix synthesis as well as a decrease in the synthesis of type I collagen and osteocalcin mRNA expression.[15] As these processes and molecules are critical for bone formation, administration of corticosteroids is disadvantageous to successful bone wound healing. Identifying a therapeutic that can be delivered to a wound site directly and reduces local inflammation would allow for proper healing of bone along with reduced malaise of the patient.

Markers of inflammation following hard tissue injury are difficult to study due to bone's mineralized composition and location deep within other tissues. As a result, healing and the associated inflammatory response following application of ACS and ACS/rhBMP-2 (or INFUSE®) therapy has yet to be fully characterized at the functional level and relies largely on patient report and gross clinical manifestations (pain and swelling).[12] Edema and erythema as a result of neovascularization may be mistaken as inflammation.[16] Preliminary data from our group and research by others have shown that genes associated with anti-inflammatory stimuli are up-regulated in response to rhBMP-2 treatment and that markers of inflammation are largely

unchanged, especially early in the healing process.[17,18] These data challenge the assumption that rhBMP-2 administration drives a greater than normal inflammatory response.

CHAPTER 2

Review of the Literature

Introduction to Bone Biology

Bone is a unique organ in that it serves several distinct functions in the body that are vital for normal physiological processes. At its fundamental level, bone provides structure and rigidity, allowing for ambulation and protection of vital internal organs. Additionally, bone functions as a storage reservoir for essential vitamins and minerals as well as the site of synthesis for cells of hematopoietic lineage. Despite its mineralized composition, bone is highly vascularized and dynamic, constantly undergoing remodeling, and is capable of complete regeneration following injury.

Bone can be classified into two main categories: lamellar (also, cortical or compact) bone or cancellous (trabecular) bone.[19,20] While these categories are distinct in form and function, the composition of bone is largely conserved. The major component of bone is bone matrix, which constitutes nearly 90% of bone volume with the remainder being filled with cells and blood vessels. Bone matrix is made up of an inorganic component (bone mineral crystals or hydroxyapatite) and an organic component (mainly type I collagen, but also types II and VII as well as glycoproteins and proteoglycans).[19] Differences in the organization of these components is the major contributor to the physical attributes of different types of bone, leading to cancellous bone possessing more flexible properties and lamellar bone being more resistant to applied force.

Typically, mature bone consists of both lamellar as well as trabecular bone.[19,21] The role of lamellar bone is to provide protection as well as a surface on which to place a mechanical load. Made up of densely packed and overlapping cylindrical units (osteons), the strength of lamellar bone is found in its compactness.[20] Alternatively, trabecular bone is hollow with a meshwork of rod-like structures randomly interspersed throughout. This hollow meshwork serves two main functions; to lighten bone and to allow space for blood vessels and marrow. Cancellous bone

makes up the majority of the epiphysis of long bone while cortical bone surrounds the hollow red marrow space of the diaphysis. In the cranium, cancellous spongey bone is sandwiched between cortical bone, providing substantial protection for the brain.[19]

A dynamic community of cells exists in and around bone. These cells originate from two distinct origins; namely from a mesenchymal stem-cell lineage (bone lining cells, osteocytes, and pre-osteoblasts/osteoblasts), or a hematopoietic stem-cell lineage (marrow monocytes and pre-osteoclasts/osteoclasts).[3,19,22] The primary cell types responsible for bone maintenance and remodeling are osteocytes, osteoblasts, and osteoclasts.[19]

The main function of osteoblasts is organic matrix deposition, but these cells also have apparent roles in homeostasis of calcium levels and osteoclast signaling.[19,22] Originating from a mesenchymal stem-cell lineage, active osteoblasts, following matrix deposition, will follow one of three cell fates: transdifferentiation into bone lining cells, differentiation into osteocytes, or cell death (apoptosis). Bone lining cells are elongated cells that lie along the bone matrix and possess extensions that contact osteocyte protrusions. These cells appear to play an important role in osteoclast recruitment and attachment through excreted enzymes that dissolve the outer layer of osteoid in response to parathyroid hormone, a signaling hormone important to blood calcium level regulation. Osteoblasts that are embedded in the ossified matrix then differentiate into osteocytes. Osteocytes reside within the mineralized bone matrix and possess cellular protrusions that interact with other cells. Osteocytes have a role in mechanical sensing and homeostatic signaling to other cells to allow for monitoring and maintenance of the surrounding matrix.

In contrast to other bone cells, osteoclasts are unique as they arise from a hematopoietic stem-cell origin. Osteoclast precursor cells are often found in the marrow and circulating blood. Active osteoclasts are characterized by having a multi-nucleated phenotype (3-11 typically) along with a large number of mitochondria and lysosomes. These cells are largely responsible for bone decomposition through localized and contained acidification at the surface of bone, resulting in

dissolution of mineralized matrix.[3] Proteases are then released to allow for the degradation of the organic matrix leading to bone resorption.

A delicate balance between all bone cells, but specifically osteoblasts and osteoclasts, contributes to the dynamic nature of bone.[23] Bone is in a continuous state of resorption and deposition. This process of bone remodeling, under normal conditions, results in no net-loss of mineralized tissue nor any change to the overall structure or function of bone.[24] Further, bone remodeling is necessary for systemic homeostasis through the tight regulation of calcium and other minerals by controlled, local release of specific hormones (i.e. parathyroid hormone, calcitonin, growth hormone, etc.).[19,25,26] The complex biological events involved in normal bone homeostasis are critically important to the innate capacity of bone to heal itself following injury.[1,2]

Bone Regeneration and Wound Healing

Fracture healing and bone regeneration is an extremely complex process involving a wide array of signaling cascades, a variety of cell types and cross talk between them, and tightly regulated timing of healing events. Healing in bone is remarkably similar to healing in other tissues with one key caveat: tissues sustaining injury will only recover about 80% of their original tensile strength during healing due to fibrotic scar formation.[27] However, under ideal conditions, bone possesses the innate capacity for complete regeneration with little to no alteration in form or function of the regenerate.

Bone wound healing falls into one of two broad categories: primary fracture healing and secondary fracture healing.[28,29] Primary fracture healing, sometimes referred to as intramembranous healing, occurs in situations where fracture margins are precisely reduced and bone heals via direct contact healing. This process closely resembles bone remolding in that osteoclasts resorb bone along the fracture line, followed by new bone deposition by osteoblasts. In cases where exact reduction does not occur, primary fracture healing may still occur through deposition of intramembranous trabecular bone followed by osteoclast-mediated remolding.

Secondary facture healing, also called endochondral healing, closely resembles endochondral ossification during bone formation [30]. This type of healing often occurs in fractures where movement and displacement of the fracture margins is present. Secondary fracture healing is characterized by a step-wise increase in fracture stability, with different forms of matrix being deposited and replaced as healing progresses. Briefly, inflammation resulting from trauma precipitates recruitment of a variety of inflammatory cells, including neutrophils and macrophages, causing initiation of healing cascades. A hematoma is formed to inhibit further bleeding. Granulation tissue is then deposited by reparative (M2) macrophages. This is later cleared and replaced by a fibrous callus laid down by fibroblasts. Chondrocytes infiltrate the fibrous matrix and the fibrous callus is replaced with a cartilaginous callus. From there, more rigidity has occurred and the process more closely resembles primary fracture healing. Osteoblasts lay down bone which is later remodeled by osteoclasts to allow for full regeneration and function. It is often the case that fracture healing does not fall into one or the other category, but is actually a combination of both primary and secondary fracture healing. **Figure 1** briefly outlines the process of endochondral fracture healing.

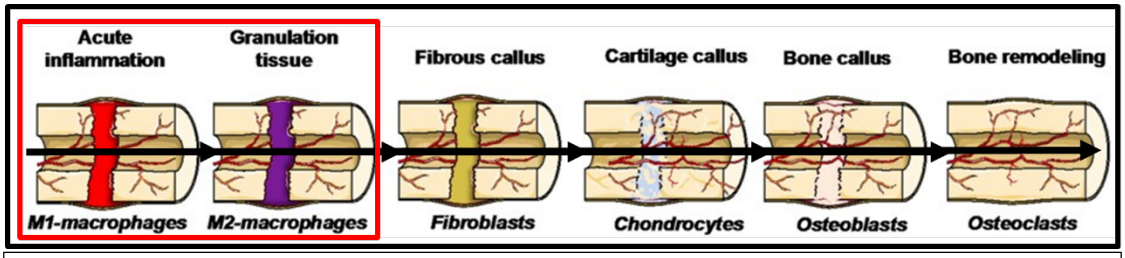

Figure1. *Steps of endochondral bone formation and associated cell types.* A variety of cell types are involved in the process of bone wound healing. Initiation of inflammation is critical in this process, followed by resolution of M1-macrophages being polarized to M2-macrophages (red box). Fibroblasts deposit a fibrous callus that is later replaced by a cartilaginous callus by chondrocytes. Osteoblasts lay down a boney callus that is later remodeled by osteoclasts to allow for complete regeneration. Figure modified from Loi *et al.* 2016.

Absolutely critical in the healing process is the correct propagation of early acute inflammation and associated signals.[2] Disruption of internal bone, periosteal, and endosteal vasculature following fracture and platelet exposition to the extravascular environment, allow for

the activation of the plasma coagulation cascade and subsequent hematoma formation.[2,31,32] Signals from damaged cells, disrupted extracellular matrix, and local tissue macrophages attract the first group of inflammatory cells, neutrophils, to the wound site within the first day of injury. Neutrophils contribute an extreme pro-inflammatory response to the fracture site, clearing tissue and secreting inflammatory cytokines (e.g. IL-6 and monocyte chemotactic protein 1 or MCP-1).[2] This initiates the second influx of inflammatory cells to the fracture site, macrophages.

Both resident bone macrophages (osteomacs) and circulating macrophages are recruited and respond to injury.[33] While somewhat controversial, macrophages are typically thought of as being activated down two specific pathways (M1-pro-inflammatory or M2 anti-inflammatory) in an event called macrophage polarization.[34] M1-macrophages, polarized by interferon- γ (INF-γ) and lipopolysaccharide (LPS), characteristically possess a caustic and often damaging "clear at any cost" phenotype.[1,2] M1's are marked by the up-regulation of inducible nitric oxide synthase (iNOS) production as nitric oxide is used both directly, to clear necrotic debris and pathogens, and indirectly, to initiate further signaling (i.e. activation of NF-κB signaling pathways).[2] Further, these macrophages secrete pro-inflammatory cytokines and chemokines, leading to positive feedback loops that continue the pro-inflammatory response. Conversely, M2-pro-repair macrophages are polarized by IL-4 and IL-13. They are characterized by the up-regulation of arginase-1 (Arg1), an important enzyme involved in collagen synthesis, along with other anti-inflammatory cytokines. Specifically, M2-macrophages secrete vascular endothelial growth factor (VEGF) and matrix metalloproteinases (MMPs), essential for matrix remodeling and angiogenesis.[16] It is important to note that terminal macrophage polarization to one specific phenotype or another has been shown definitively *in vitro* but is much more difficult to show *in vivo*.[1,2,34,35] Instead, macrophages found *in vivo* tend to fall on a spectrum, possessing phenotypical characteristics of both M1 and M2 macrophages.[34] **Figure 2** is a simple schematic outlining macrophage polarization[36].

Early macrophage response to a fracture most closely resembles the classical M1 pro-inflammatory macrophage response to damage and necrosis. The fracture environment is characterized by an array of inflammatory cytokines (TNF-α, IL-1ß, IL-6, MCP-1, IL-12) and a clearing of matrix and necrotic cells via phagocytosis, often causing a degree of further tissue damage.[1,2,33] Release of these cytokines also contributes to osteoclast activation that initiates the resorption of necrotic bone. This inflammatory cascade activates some of the earliest signaling pathways that will be used to initiate repair via the recruitment of fibroblasts (FGF), stem cells (SDF-1), and osteoprogenitor cells.[19,28]

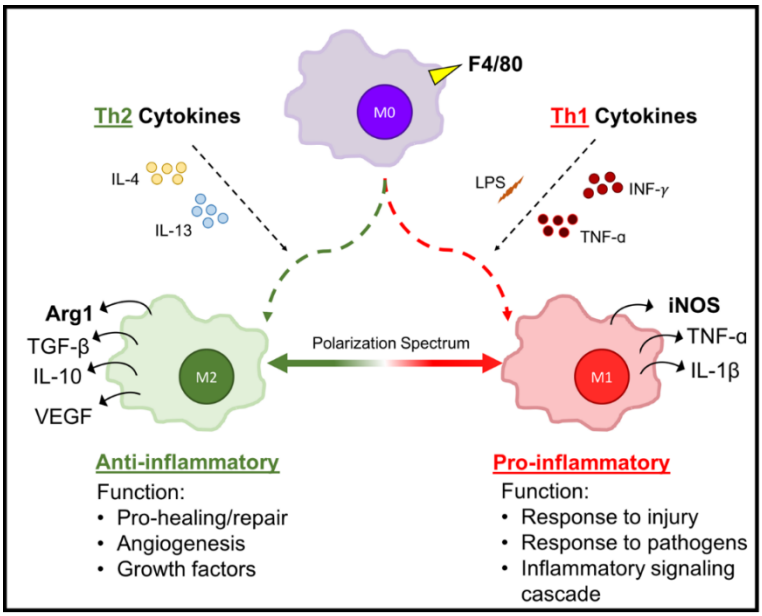

Figure 2. *Macrophage polarization.* Macrophages express several surface markers. One of the most common markers of macrophages is F4/80. The un-polarized (M0) macrophages can be guided down two main paths, dependent on the exogenous signals that are received. Pro-inflammatory cytokines and factors (lipopolysaccharide, INF-γ, TNF-α) direct macrophages down the classical M1 pathway. These macrophages are responsible for responding to injury and pathogen invasion and are characterized by the production of NO as well as other inflammatory cytokines. Conversely, alternatively activated macrophages (M2) are polarized by ant-inflammatory cytokines (IL-4, IL-13) and have functions in healing and angiogenesis. It is important to note that polarization is usually not definitive and is a spectrum, with macrophages generally expressing at least some degree of both phenotypes. Figure modified from Johnson, 2012.

Within several days to a week, clearing of necrotic cells has ceased and M2 macrophages have begun the process of granulation tissue deposition, along with initiating inflammation termination. In addition to being polarized by anti-inflammatory cytokines, M2-macrophages respond to the by-products of tissue damage and cell debris, leading to further reductions in inflammation. Secretion of growth factors (i.e. TGF-ß, VEGF) and deposition of matrix allows for the early stages of repair to begin, and thus, M2-macrophages are often considered to have a

pro-healing and repair phenotype. This activation propagates the next stages of healing seen in **Figure 1**.

While bone possesses the innate capacity for complete and contiguous regeneration, this is highly dependent on the degree of injury and proximity of the fracture margins to each other. Injury and trauma resulting in large portions of ablated or disarticulated bones pose a serious issue for medicine.[14,28,31,32] Individuals sustaining large injuries, or who are subject to the iatrogenic removal of large portions of bone, may have difficulty in the spontaneous regeneration of bone, particularly if the individual is under an impaired health status or metabolic restriction. In these cases, clinical intervention is necessary.

Clinical Interventions

Several bone tissue engineering strategies have emerged over the last several decades in order to alleviate the burden associated with surgical and fracture non-unions.[8,37] A major approach of this initiative is to provide a therapeutic that contains both an osteoconductive matrix, on to which bone repair and remodeling cells can adhere, along with an osteoinductive mechanism that provides signaling to bone forming cells to initiate and/or heighten the healing response.

Currently the "gold standard" intervention in the field of bone regeneration is the autologous bone graft. In these surgeries, a piece of bone isolated from a section of the patient's healthy bone (i.e. the ramus of the mandible or the iliac crest) and is implanted into the non-union wound site.[4-6] As this bone possesses all of the same immune markers as the patient, this intervention has been very successful on the basis that there is little risk of rejection.[4] Furthermore, the graft, being living bone, is both osteoconductive and osteoinductive, providing bone matrix on to which osteoprogenitors can attach along with all of the signaling factors innate to actively remodeling bone. Despite the successes and positive clinical outcomes, autologous bone grafting does not provide an ideal clinical intervention due to the co-mrobidity of a second

surgical site and is limited by tissue available for harvest; thus necessitating research in alternative means of bone tissue engineering.[7,9,11,29,37,38]

Several strategies have been investigated to ameliorate the problems associated with autologous grafting, namely adjunctive cell therapy, implantation of biomaterials and scaffolds, and manipulations of osteogenic signaling pathways. One such therapy that has become particularly popular is the use of the INFUSE® Bone Graft (Medtronic, Menneapolis, MN). INFUSE® is a combination therapy delivering osteoinductive *recombinant human bone morphogenetic protein-2* (rhBMP-2) on an osteoconductive absorbable collagen sponge (ACS) scaffold. Currently, INFUSE® is U.S.-Food and Drug Administration (US-FDA) approved for four clinical indications: two oral-maxillofacial procedures (sinus lifts and ridge augmentations), tibial shaft fractures, and spinal fusions. Despite the limited indications, rhBMP-2 (INFUSE®) is still widely used in a variety of clinical applications from pediatric cleft palate procedures to repair of iatrogenic defects following malignant bone neoplasm. Indeed, over 90% of rhBMP-2 administration is within the confines of an off-label application.[11,39] Though rhBMP-2 has been used to make great strides in the areas of bone tissue regeneration and healing augmentation, recent controversy concerning the use of this product has brought into question its efficacy. Specifically, uncertainties about regenerate integrity as well as adverse side effects associated with treatment leading to poor healing outcomes have been cited.

Adverse Side Effects with rhBMP-2

Endogenous BMP-2 signaling is necessary for proper activation of osteoblasts and subsequent deposition of bone. BMP-2 signaling is mediated via Smads (typically Smad 1, 5, and 8). Binding of BMP-2 to BMP receptors results in translocation of hetero-smad dimers to the nucleus, resulting in induction of runt-related transcription factor 2 (Runx2), a key transcription factor involved in osteogenic programming.[19,40,41] However, the addition of supraphysiological dosing of exogenous BMP-2 results in damaging and potentially dangerous events associated with bone healing and remodeling, often leading to therapeutic failure.

A wide panel of reported adverse clinical side effects associated with rhBMP-2 administration exists in an ever growing body of literature aimed at exploring conditions under which this therapeutic fails.[12,13,17,18,42-45] While rhBMP-2 results in robust bone deposition following administration, the quality of the regenerate is often questionable, with bone that is excessively porous compared to native bone and bone that fairs poorly in biomechanical testing. As a result of these trademark characteristics, this type of bone is termed "BMP bone". Not only is the bone of poor quality, but often the bone grows in places that are not contiguous with the native bone. Ectopic bone formation occurs in greater than 70% of patients receiving rhBMP-2, a rate that is nearly six times that of patients not receiving rhBMP-2.[46] Though the reasons for this disparity are understudied, it is known that a larger portion of administered rhBMP-2 is released out and away from the wound bed, likely activating cells sensitive to BMP signaling to initiate osteogenic signaling pathways. Therefore, the investigation into novel delivery mechanisms of rhBMP-2 delivery is critical to the success of this powerful peptide in the clinical setting.

Another side effect associated with the delivery of rhBMP-2 is activation of osteoclasts and subsequent osteolysis. It is well established that, in cancellous bone, BMP-2 enhances osteoclast activity. It has been shown by multiple independent studies that rhBMP-2 administration can result in significant increases in osteolysis, particularly in procedures of the spine. Additionally, rhBMP-2 delivery has been shown to promote adipogenesis, resulting in lipid deposition within the trabecular space of bone, leading to the formation of bone cysts.[12,47]

While rhBMP-2 administration has been associated with urogenital problems as well as with a risk of tumor formation,[48-50] more attention has been paid to the role of rhBMP-2 in increasing inflammation and furthering wound complications. From benign seroma formation to life threatening cervical spine swelling, significant side effects associated with local inflammation secondary to rhBMP-2 administration have been noted. In fact, the FDA released a black box warning against the use of rhBMP-2 in the cervical spine in 2008 on the account of six fatalities reported with this off-label use.[39] Studies have also reported a greater than 3000-fold increase in

IL-6 and 34-fold increase in TNF-α levels in the seromas of subjects treated with rhBMP-2,[51] further raising questions about the potentially caustic effects of heightened and prolonged inflammation. In addition to inflammation, infections in patients receiving rhBMP-2 have been shown to be significantly more common than in control populations and several studies have shown the rate of general wound complications to be nearly double that of normal patients with this therapeutic.[52]

Several remedies have been studied to ameliorate the side effects associated with rhBMP-2. In the area of inflammation, one avenue of study is the systemic delivery of anti-inflammatories. Using non-steroidal anti-inflammatories (NSAIDs) or corticosteroids could certainly off-set the heightened inflammation reported with rhBMP-2 use, but this comes at the cost of dampening innate immune responses to subsequent injury or infection while undergoing treatment. Additionally, corticosteroids are contraindicated for patients with fractures as their use has been associated with a decrease or delay in bone wound healing. Corticosteroids have been shown to induce apoptosis of osteoblasts and osteocytes as well as prolong the lifespan of osteoclasts.[15] Further, corticosteroids have been shown to decrease the synthesis mRNA for type I collagen, a major component of bone matrix, and osteocalcin (BGLAP), a protein critical to bone building and mineralization.[15] These combined effects are disadvantageous to successful bone wound healing. Alternatively, specific local administration of an anti-inflammatory, whether loaded onto the rhBMP-2 carrier or as an intrinsic property of the scaffold itself, may hold a valuable key in better harnessing the power of exogenous BMP-2 administration.

pGlcNAc Nanofiber Scaffolds

The key to local anti-inflammatory stimuli following bone wounds may be found in alternative scaffolding that could locally reduce inflammation and provide for a more controlled release of rhBMP-2. US-FDA approved pGlcNAc (short poly-N-acetyl glucosamine or sNAG, Talymed®), a marine diatom-derived polysaccharide nanofiber scaffold, has gained interest as it has been shown to aid in the healing of cutaneous wounds.[53-56] This novel nanofiber scaffold is an

appealing candidate for bone healing as it has been shown to reduce scar formation, increase tensile strength of the regenerate, align collagen fibers and reduce inflammation, promoting faster healing in a skin wound model.[54] Further, pGlcNAc has been shown to promote angiogenesis in skin wounds via activation of the Akt1(protein kinase B, PKB) signaling pathway.[55] The pro-healing effects of pGlcNAc may provide an effective mechanism that could be a valuable tool in delivering local, controlled anti-inflammatory activity to counteract that of rhBMP-2. Additionally, recent preclinical data from our lab on the release kinetics of rhBMP-2 from pGlcNAc indicate that this scaffold may be more efficacious in binding rhBMP-2 than ACS, mediating some of the problems of ectopic bone formation. Understanding how pGlcNAc modulates inflammation response in bone could provide further understanding of how to design a combinatory therapy for bone wound healing.

Preclinical Animal Model

The complexity of inflammation and healing necessitates an *in vivo* animal model to investigate inflammatory symptomology at the gross and molecular level. While non-human primates and other large mammals provide a model that may be more directly translatable to human disease, logistical complexities as well as lack of molecular assays for these models make this avenue particularly undesirable. Mice and rats have long been a staple in laboratory research, providing a model that is inexpensive, consistent, and lends itself to common and available molecular strategies.

Several murine bone healing models exist in these animals. The closed three point tibial fracture model is a commonly used model to test fractures in the appendicular skeleton but is limited in the ability of the investigator to precisely control the fracture, which becomes especially crucial when comparing results and observations between animals. Another commonly used appendicular fracture model is the femoral osteotomy. While the strength of this model is consistent and comparable between wounds, the model is limited procedurally, as rodent osteotomies are time consuming and labor intensive. The critical sized calvarial defect model

takes several strengths from the aforementioned bone healing models while also addressing the major weaknesses.

The murine calvarial critical sized defect is a well-established preclinical model that has been used in bone research for well over the last twenty-five years.[17,57-64] A critical sized defect (CSD) was defined by Schmitz and Hollinger (1986) as the smallest interosseous defect that will not spontaneously heal during the life of the animal.[63] While it is somewhat debated in the literature, it is generally accepted that a greater than 5 mm defect in the mouse calvaria is critical sized.[57] The murine CSD model has been used in a wide assortment of bone related research, specifically in the areas of tissue engineering and repair strategies. Defects can be made in the calvaria with precise consistency, allowing researchers to apply a quantitative approach to downstream analysis. Specific to our interest, the mouse CSD model allows for a cost effective, high throughput, and controlled approach to *in vivo* investigation of fracture healing. Surgeries are rapid and animals are able to make an expedient recovery with little risk of post-operative complications. Further strengthening this model, calvarial bone is similar to maxillary and mandibular bone, making it an ideal model for investigating rhBMP-2 driven healing, as two of the clinical indications for this therapy are oralmaxillofacial in nature. As such, the mouse calvarial CSD is the ideal model for the purposes of this investigation.

CHAPTER 3

Significance

Currently, INFUSE® is a common therapeutic used in the treatment of traumatic or surgical bone loss[65]. Despite its widespread use, the underlying mechanisms for the frequent surgical failures following treatment have yet to be elucidated. One promising avenue is in the area of inflammatory dysregulation. This present study provides a baseline characterization of the inflammatory response and morphological changes with ACS application during the acute phase of bone wound healing. Furthermore, the study outlines the effect that bone morphogenetic protein-2 administration has on modulating these inflammatory pathways as well as the role that the therapy has in neovascularization and healing. Finally, this study establishes a platform for developing therapies to better treat bone wounds in the future through a combinatory therapy of INFUSE and pGlcNAc. Better understanding of the mechanisms by which ACS, rhBMP-2, and pGlcNAc regulate inflammatory processes will likely inform future novel pharmacological avenues that could be used for patient benefit.

Hypothesis

We hypothesize that delivery of rhBMP-2 will result in increased inflammation as evidenced by a prolonged M1-macrophage response, a delayed M2-macrophage response, and increases in angiogenesis, presenting clinically as erythema. Further, it is predicted that the administration of a pGlcNAc nanofiber scaffold will result in the local reduction of inflammation at the wound site.

Specific Aims

The specific aims of this murine calvarial defect study are to:

a) Characterize healing morphology and acute inflammation of ACS application to an iatrogenic bone wound.

b) Interrogate how wound healing morphology and inflammation are altered through the use of growth factor (rhBMP-2) and a novel scaffold (pGlcNAc woven nanofibers).

CHAPTER 4

Materials and Methods

Methods Overview

Calvarial defects (5mm) were created in eighty-four 8 week old C57BL6 mixed sex, wild-type mice. Defects were immediately treated with either ACS alone (control), ACS loaded with rhBMP-2, or a pGlcNAc nanofiber scaffold. Mice were sacrificed at 3 and 7 days post-operation and calvarias were isolated for downstream analyses. A portion of isolated calvarias were paraffin embedded for histological analysis while an 8 mm biopsy of tissue surrounding the defect on the remaining calvarias was performed for protein extraction. Isolated protein was subjected to inflammatory cytokine arrays and western blotting. Mounted tissue sections were stained with hematoxylin and eosin for morphological characterization within the defect. Further, immunohistochemistry for markers of inflammation and macrophage polarization were performed and analyzed for effects on inflammation and tissue repair.

Animals

Eighty-four mixed sex C57BL6 wild type mice (*Mus musculus*), age 8 weeks, weight 16-25g, were purchased from Jackson Laboratory (Bar Harbor, ME). Upon arrival, animals were allowed to acclimate in plastic cages for one week prior to the start of surgery. Animals were housed 5 per cage, segregated by sex, with *ad libitum* access to water and a regimented laboratory diet. Cages were kept in a temperature and humidity controlled room within an Association for Assessment and Accreditation of Laboratory Animal Care International accredited facility where husbandry and related services were provided by the Division of Laboratory Animal Resources for the duration of the study. The Medical University of South Carolina Institutional Animal Care and Use Committee approved all Animal Use Protocols (AR3452). All procedures and the reporting thereof are in compliance with the Animal Research: Reporting in VivoExperiments (ARRIVE) guidelines.[66]

Biomaterials

Scaffold preparation was performed in a sterile laminar flow hood. ACS (Helistat® Absorbable Collagen Sponge, Integra Life Science, Plainsboro, NJ, USA) punches were made using a 6 mm biopsy punch and stored in a sterile 24 well plate atop sterile gauze. Likewise, pGlcNAc nanofiber scaffold (Talymed® Marine Polymer Technologies, Inc., Danvers, MA) punches were made using a 5 mm hole punch and stored in a sterile 24 well plate atop sterile gauze. Plates were stored at room temperature. rhBMP-2 (INFUSE® Bone Graft, Medtronic, Menneapolis, MN) was prepared according to manufacturer's direction and reconstituted at a concentration of 1 µg/µL, which was kept frozen until time of surgery. At time of implantation, the stock solution of rhBMP-2 was diluted to a concentration of 0.013 µg/µL in sterile water and 25 µL was soak loaded onto the ACS punch (325ng of loaded protein) and allowed to bind at room temperature for 15 minutes (as per instruction), during which the ACS punch would shrink to a diameter of 5 mm. Control ACS was loaded with 25 µL of sterile water. pGlcNAc was loaded with 1.1 µL of sterile water (difference based on saturation limit of each biomaterial). Loading schema available in **Table 1**.

Table 1. Loading schema by treatment group.

Treatment Group	Water (µL)	13 µg/mL rhBMP-2 (µL)
ACS only	25	0
ACS + rhBMP2	0	25
pGlcNAc	1.1	0

Experimental Design

Animals were organized by cage and sex to be evenly distributed into three experimental groups (ACS only, ACS + rhBMP-2, or pGlcNAc only) and two healing time points (3 or 7 days). This experimental schema allowed for fourteen animals in each group with seven males and seven females each. 325ng of rhBMP-2 was chosen based on previous data from the lab suggesting this amount resulted in the best healing outcomes at four and eight-week time points. Groups are outlined in **Table 2**.

Table 2. Animals per treatment groups by day, sex, and processing method.

Treatment Group	3 day	7 day	Specimen Processing
ACS only	8 (4M/ 4F)	8 (4M/ 4F)	Protein
	6 (3M/ 3F)	6 (3M/ 3F)	Histology
ACS + rhBMP-2	8 (4M/ 4F)	8 (4M/ 4F)	Protein
	6 (3M/ 3F)	6 (3M/ 3F)	Histology
pGlcNAc only	8 (4M/ 4F)	8 (4M/ 4F)	Protein
	6 (3M/ 3F)	6 (3M/ 3F)	Histology

Surgical Procedures

Surgery preparation, surgeries, and, recovery were performed in the same room under the guidance of a team of experienced researchers. Animals were anesthetized individually with isoflurane and O_2 in an induction chamber. Following induction, the animal's head was shaved and a 10% providone-iodine solution was used as an antiseptic with careful attention taken to avoid contact with the eyes. The antiseptic was then wiped off with 70% ethanol. This was repeated two more times before the animal was given a unique ear punch identifier. Animals were given an analgesic (Carprofen, 2.5mg/kg) for post-operative pain via subcutaneous injection. Prior to moving to the surgical field, an ocular lubricant was added to each eye to prevent excessive drying during the surgery.

All surgeries were performed by an experienced surgeon (RNH, JC). The animal's head was placed on a stereotaxic device with a nosecone delivering isoflurane and O_2. A toe pinch was preformed to ensure proper anesthesia was administered. A 10-15 mm sagittal incision was made along the midline of the calvarium. Soft tissue of the skull was reflected and the periosteum was removed. A craniectomy was preformed using a 5 mm trephine and a slow-speed hand drill along the mid-sagittal suture. Special care was to taken to insure that the dura mater was not damaged. Where bleeding occurred, sterile gauze and pressure were applied until bleeding was stopped before continuing. Next, depending on experimental group, the appropriate scaffold (following incubation and all technical guidelines) was loaded into the center of the defect (**Figure 3**). Soft-tissue margins were approximated and the wound was closed with 6/0 polypropylene sutures. Animals were moved to a recovery cage on a heated pad until ambulant, upon which they were moved to a clean cage.

Figure 3. *Methodological workflow of surgical procedure.* Mice were anesthetized, scalps shaved and sterilized, and a midline scalp incision was made exposing the skull and allowing for trephination (A). A 5mm trephine was used to create the critical sized calvarial defect (B). Careful attention was payed to not disturb the underlying dura mater and the defect was removed (C). Administration of the scaffold (ACS or pGlcNAc) was applied to the defect area (D).

Animals were monitored daily for appearance, weight, activity, and any signs of pain. Additional dosages of carprofen were administered where necessary. Any treatment and abnormality was documented in the surgical log.

Euthanasia

Euthanasia was preformed 3 and 7 days post-operation via CO_2 asphyxiation (primary) and cervical dislocation (secondary). Animals were divided into groups based on downstream analysis. The animals were then decapitated and soft-tissue was removed from the skull. For specimens used in protein extraction, an 8 mm biopsy of tissue around the defect and regenerate was taken and placed in PBS on ice. For histological specimens, the calvaria was removed, careful to leave any unabsorbed scaffold in place, and placed 3.7% formalin.

Protein Extraction

Immediately following euthanasia, the 8 mm biopsy punches for protein extraction were cut into smaller pieces, wrapped in aluminum foil, and pulverized with a liquid nitrogen cooled mortar and pestle. Homogenate was transferred to a centrifuge tube containing 300 µL of RIPA buffer and agitated for two hours at 4°C. Following agitation, tubes were centrifuged for 20 minutes at 12,000 rpm at 4°C. The supernatant was removed and placed into a new tube. The Pierce™ BCA Protein Assay Kit was used to calculate protein concentrations for downstream analysis. Samples were stored at -80°C.

Tissue Processing

Calvariae assigned to histological analysis were allowed to fix in 3.7% formalin for 48 hrs. Following fixation, specimens were transferred to 70% ethanol for 24 hrs, then moved to a 0.25 M ethylenediaminetetraacetic acid (EDTA) solution at pH 7.4 for decalcification. EDTA was replaced every 3-4 days and decalcification was monitored. At regular intervals, samples were pierced with a twenty-one gauge hypodermic needle and resistance was noted. Samples were allowed to decalcify for 3-4 weeks, upon which it was determined that the samples had sufficiently decalcified for further processing. Following decalcification, specimens were coronally bisected through the center of the defect, resulting in a posterior and anterior portion. Specimens were transferred to 70% ethanol for short term storage.

Samples were processed overnight on a Tissue Tek® VIP tissue processing machine. Briefly, whole calvarias were individually placed in embedding cassettes, then placed into the tissue processor. Specimens were washed, dehydrated in graded ethanol (70-100%), cleared in xylene, and infiltrated with paraffin. Immediately following overnight processing, samples were embedded in paraffin wax. Bisected pieces of the same specimen were embedded in a single block, defects towards the front of the mold at a 90° angle to the face. Blocks were cooled on a cooling table and stored at room temperature until sectioning occurred.

Paraffin embedded specimens were sectioned on a Microm® HM 340 E rotary microtome. For sectioning, blocks were mounted into a microtome chuck and the surfaced was planned until the first sections with tissue present emerged. 7 µm serial sections were cut, carefully transferred and floated in a 35-40°C water bath, and mounted on slides. Two to three sections were mounted on each slide and a minimum of 30 slides were cut for each sample. Slides were dried overnight in a 37°C oven before being transferred to slide boxes for storage at room temperature.

Histology

Blinded representative samples from each group and time point were selected for downstream analysis (n=4). Three slides from each sample, at least 40 µm apart, were chosen and placed randomly into staining trays, leaving an empty slot between slides to allow for appropriate penetration of stains and reagents. This procedure was repeated for each subsequent stain (H&E and IHCs).

Hematoxylin and Eosin Staining

Slides were stained following a standard Harris' Hematoxylin & Eosin staining protocol. Staining times and conditions were optimized to provide for the best staining. Briefly, slides were deparaffinized in xylene, rehydrated in graded ethanol (100-70%) then placed in diH_2O. Slides were then stained in Harris' hematoxylin for 10 minutes, returned to running tap H_2O for 8 min, quickly clarified, and stained with eosin for 1 minute. Following staining, slides were dehydrated

once more in graded ethanol (70-100%) then moved to xylene. Stained slides were mounted with permount and allowed to dry overnight at room temperature. Whole defects were imaged at 10x magnification using a Motic Inverted Microscope with attached camera (Motic, British Columbia, Canada) and stitched together using Image Composite Editor (Microsoft®, Redmond, WA) for further downstream analysis.

Stitched 10x images were subjected to cell count analysis to assess relative differences in cell number and infiltration in the healing defect. The ImageJ Deconvolution pluggin was used to separate hematoxylin stained nuclei from other tissues. Color was converted to a binary white/black color scheme for analysis. Particle size parameters were set to minimize background and the number of particles, representing cell nuceli, was quantified. An additional normalization calculation was performed by comparing nuclei counts to the total area counts.

Immunohistochemistry

Immunohistochemistry for a pan-macrophage marker (F4/80; PA5-32399, Thermo Fisher Scientific, Waltham, MA), inducible nitric oxide synthase (iNOS; ab15323, Abcam, Cambridge, MA), arginase-1 (Arg1; PA5-29645, Thermo Fisher Scientific, Waltham, MA), and platelet endothelial cell adhesion molecule (PECAM; ab28364, Cambridge, MA) for vessel formation, were performed (**Table 3**). iNOS is classically associated with a M1, pro-inflammatory macrophage phenotype while Arg1 is classically associated with repair and an M2, pro-healing macrophage phenotype. PECAM was chosen as a marker of angiogenesis associated with repair.

Slides were deparaffinized in xylene, rehydrated in graded ethanol (100-70%), and placed in diH_2O. Slides were then blocked for 10 minutes in 3% hydrogen peroxide in methanol to block endogenous peroxidase activity. Samples were washed in PBS and covered for an additional 10 minutes with 1% goat serum and 1% bovine serum albumin to block non-specific binding. Primary antibodies (see above) were diluted and added to sections. Incubation occurred overnight at 4°C. The next morning, slides were washed with PBS and incubated with a secondary antibody (Goat anti-rabbit IgG; ab6721, Abcam, Cambridge, MA) at a dilution of 1:250 for one hour at

room temperature. Slides were again washed with PBS. Diaminobenzidine (DAB; Vector Laboratories, Bulingame, CA) detection method was used to detect immunoreactivity. DAB was prepared according to manufacturer's instructions and allowed to incubate on sections until brown immune reactivity was observed (approximately 30 seconds to 4 minutes). DAB activity was neutralized in diH_2O. Slides were counterstained in diluted Harris' hematoxylin (diluted 1:1 in diH_2O) for orientation and serially dehydrated before being moved back to xylene. Slides were mounted with permount and allowed to dry overnight at room temperature. Specific DAB incubations times and dilutions can be found in **Table 3**.

Table 3. Use specification of antibodies used in IHC.

Antibody	**Catalog Number**	**Primary Dilution**	**DAB Incubation Time**
F4/80	PA5-32399 (Thermo)	1:100	2 minutes
iNOS	ab15323 (Abcam)	1:100	4 minutes
Arg1	PA5-29645 (Thermo)	1:350	45 seconds
PECAM	ab28364 (Abcam)	1:50	40 seconds

Immunohistochemistry Data Analysis

Representative images taken from slides stained for immunohistochemical markers were subjected to quantitative analysis for presence and intensity of positive staining. Briefly, representative 10x images were taken at the both surgical margins and the center of the defect, resulting in three images for each slide. Images were compared by Image J Software and the IHC Profiler Open Source Plugin for automated scoring of immunohistochemical staining to quantify percent positivity. At least three sections per individual and per target were analyzed. Data were averaged by group, graphed, compared by treatment and time, and subjected to statistical analysis.

Specific to PECAM immunohistochemistry, a sub-analysis was performed to interrogate regional healing within the defect. For this analysis, three unique regions of interest were chosen (sinus related, non-sinus related, and surgical margin). An H&E indicating the regions of interest can be seen in **Figure 4**. Image J was used to draw a 300 x 300-pixel box in these three locations. As before, IHC profiling was performed on the newly defined region of interest for all samples. Data were averaged and graphed and subjected to statistical analysis.

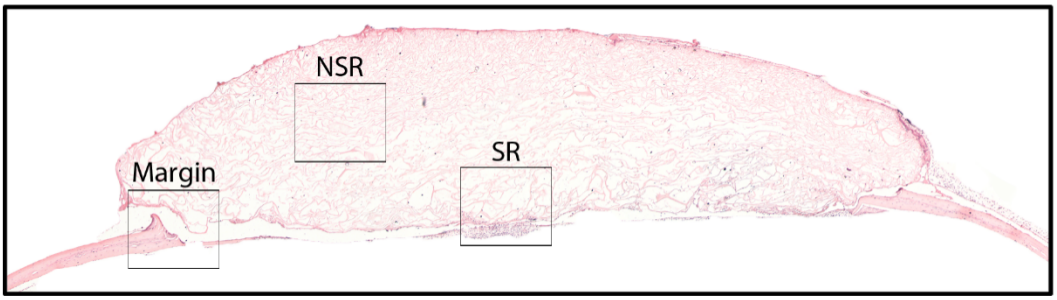

Figure 4. *Regions of interest chosen for regional assessment of PECAM expression.* Three regions of interests were selected to evaluate if there was a sub-localization of healing, indicated by PECAM expression. Margin=surgical margin, NSR=non-sinus related, SR=sinus related. H&E stained section for orientation.

Western Blotting

Standard western blotting methodology was used to interrogate specific targets of interest selected based on preliminary cytokine data. Antibodies for specific targets and working dilutions can be found below in **Table 4**. Calculations were performed to normalized protein concentrations across samples and time points based on previously performed BCA assays. TGX Fast Cast Stain Free Acrylamide Gels (Bio-Rad Laboratories, Hercules, CA) were poured and allowed to polymerized according to manufacturer's instructions. Protein isolated from the calvarial defect was thawed and diluted in diH_2O. 4x Laemmli Sample Buffer (Bio-Rad) and 2-mercaptoethanol were added to the sample to allow for protein denaturing and consistent running. Samples were heat denatured at 100°C for 5-15 minutes. Previously poured gels were placed into a gel holding apparatus and filled with running buffer. Samples were added to the appropriate wells of the gel, along with a ladder (Precision Plus Protein™ All Blue Prestained Protein Standards, 1610373, Bio-Rad Laboratories, Hercules, CA) for appropriate identification of the

targets. Three individuals from each group were selected and run on three separate gels, with appropriate controls and treatments on each gel (n=3). Gel electrophoresis proceeded at 300 volts for approximately 30 minutes, dependent on the size of the target protein.

Following electrophoresis, gels were carefully removed from the gel cassette, placed on a UV light box, and activated for 5 minutes. Visualization of the activated protein was captured on a Syngene G:Box XX6 (Biocon, Syngene International, Bengaluru, India). After activation, gels were placed in a transfer sandwich with nitrocellulose transfer membrane and transfer proceeded. Transfer was performed in cold transfer buffer at 90 volts for 90 minutes. Following transfer, membranes were imaged on the G:Box to verify transfer efficacy. Membranes were then transferred to 5% lab grade milk blocking buffer dissolved in tris-buffered saline and tween 20 (TBST) and allowed to block for one hour at room temperature, with agitation. After blocking, membranes were washed five times with TBST. Primary antibody dilutions were optimized for each specific target antibody. Primary antibodies were diluted in 5% milk block and added to membranes. Membranes were incubated with primaries overnight at 4^{o}C with agitation.

Table 4. Use specifications for antibodies used for western blotting.

Antibody	**Catalog Number**	**Primary Ab Dilution**	**Secondary Ab Dilution**
VEGF-A	ab46154 (Abcam)	1:1000	1:3000
IL-17	ab79056 (Abcam)	1:1000	1:3000
MCP-1	ab25124 (Abcam)	1:1000	1:3000
TNF-α	ab6671 (Abcam)	1:250	1:3000

After overnight incubation, membranes were washed five times with TBST. Secondary antibody (Goat anti-rabbit IgG, ab6721, Abcam, Cambridge, MA) and ladder conjugate (Precision Protein^{TM} StepTactin-HRP Conjugate, Bio-Rad Laboratories, Hercules, CA diluted

1:3000) were prepared at a concentration that was optimized for each target (**Table 4**). Secondary antibody and ladder conjugate were added to the membrane and allowed to incubate for 1 hour. Following secondary antibody incubation, membranes were washed once with a high salt buffer wash (29.22% w/v NaCl, 0.2% w/v KCl, 3.0% w/v Tris, 2% v/v Tween 20, pH 7.4) and then five times with TBST. Clarity™ Western ECL Blotting Substrate (Bio-Rad Laboratories, Hercules, CA) were used to detect target bands. ECL reagent was prepared according to manufacturer's instruction and added to the membrane. Membranes were allowed to incubate for 5 minutes at room temperature. ECL reagent was removed and replaced with TBST before being imaged on the G:Box.

Recombinant mouse protein for certain targets were obtained to verify the level of detection of the western blots (**Table 5**). Lyophilized protein was reconstituted in diH_2O at a concentration of 25 µg/mL. Serial dilutions were performed in order to load between 400 ng and 0.004 ng of protein per well. The same blotting methods as before were followed to accurately determine detection levels in our system.

Table 5. Recombinant mouse protein used for western blot limit of detection analysis.

Mouse Recombinant Protein	Catalog number
rmIL-17	ab50162 (Abcam)
rmTNF-α	ab9740 (Abcam)
rmMCP-1	ab9901 (Abcam)

Western Blotting Data Analysis

Blot images captured on the G:Box were analyzed using Bio-Rad's Image Lab™ Software. Stain free total protein blot images were used to normalize protein concentration intensity and correct for loading error. Image Lab™ was then used to quantify band intensity for each sample. Biological triplicates were averaged and graphed where appropriate. Data was subjected to statistical analysis to determine significance, if any.

Statistics

Student's t-tests and two- or three-way Analysis of Variances (ANOVAs) with post-hoc Bonferroni analyses were conducted for all comparison where appropriate. Violations of homogeneity of variance and normality were corrected through transformations of the data where needed. Differences were considered significant where $p \leq 0.05$. All data are presented as means ± standard error of the mean (SEM).

CHAPTER 5

Results

Summary

Overall, rhBMP-2 administration of 325 ng resulted in no observable change in the gross morphology of the mouse calvaria compared to ACS alone (e.g. no clinical signs of inflammation). Similarly, pGlcNAc administration resulted in no observable change in the gross morphology compared to ACS alone. Histological investigation showed a marked increase in fibroblastic cellular infiltrate into the wound site with subclinical rhBMP-2 administration compared to ACS control. While there was an increase in cellular infiltrate with rhBMP-2, data showed that there was a delay in macrophages recruited to the wound site. Further, these macrophages were not polarized to one specific phenotype. Conversely, pGlcNAc administration resulted in compactness of the cellular infiltrate phenotype and pathological scoring showed what appeared to be a caustic neutrophilic environment. pGlcNAc increased M1-like macrophages early, albeit not significantly. Resolution to baseline levels occurred by seven days with treatement. Data indicated that both rhBMP-2 and pGlcNAc administration had no significant effect on angiogenesis, though both showed downward trends in VEGF-A expression when compared with the ACS control group.

Gross Observations

Mice observed following surgery showed no gross, obvious signs of increased inflammation with ACS treatment, pGlcNAc treatment, or ACS/rhBMP2 treatment. Furthermore, at time of sacrifice, no notable observations concerning inflammation were made. While rhBMP-2 is often cited as producing ectopic bone growth,[12,13,67] no ectopic bone growth was noted at these early times of sacrifice.

Histological Analysis

Hematoxylin and Eosin Stain

Hematoxylin and eosin stained sections of defect containing ACS alone provided a baseline starting point for general observations to be made and data to be collected about early inflammatory changes from three to seven days. Careful observation of control ACS group at three days showed very little cellular infiltrate into the wound site. The ACS scaffold remained largely de-cellularized, even at the base of the scaffold closest to the underlying dura mater. Cell presence, marked by hematoxylin stained nuclei, was reserved almost exclusively to the underlying dura and cells of resident bone. Along the dura in most samples was a clearly defined cluster of cells directly in the middle, congruent with the sagittal sinus. The ACS scaffold itself, being comprised of collagen, readily took-up the eosin dye and stained in a similar fashion to bone. Surgical margins of the bone were clearly defined and contrasted well with the unorganized structure of the scaffold. Largely, little regenerate was present within the surgical site with this treatment at this time point (**Figure 5A**).

By seven days, cellular infiltration was noticeably increased compared to the three day time point. While cell abundance within the ACS matrix remained relatively low, cells in and around the dura appeared to have proliferated and continued to migrate ectocranially into the scaffold. The depth of infiltrate had thickened to become as thick or thicker than the resident bone on either side of the defect. Surgical margins were still clearly distinguishable from the unorganized matrix as well as the cellular infiltrate. New fibrous matrix deposition was visible where cellular infiltrate was most abundant. The ACS scaffold appeared to be completely intact, with no obvious signs of decomposition. Cells were present at the top of the matrix, likely infiltrating from the dermis of the scalp. The center of the ACS was still largely acellular (**Figure 5A**). Cell counts from three and seven day ACS control samples revealed that there was no significant increase in cellular infiltrate between three and seven days. However, it should be noted that, despite the lack of statistical difference, there was a more than 42% increase in the

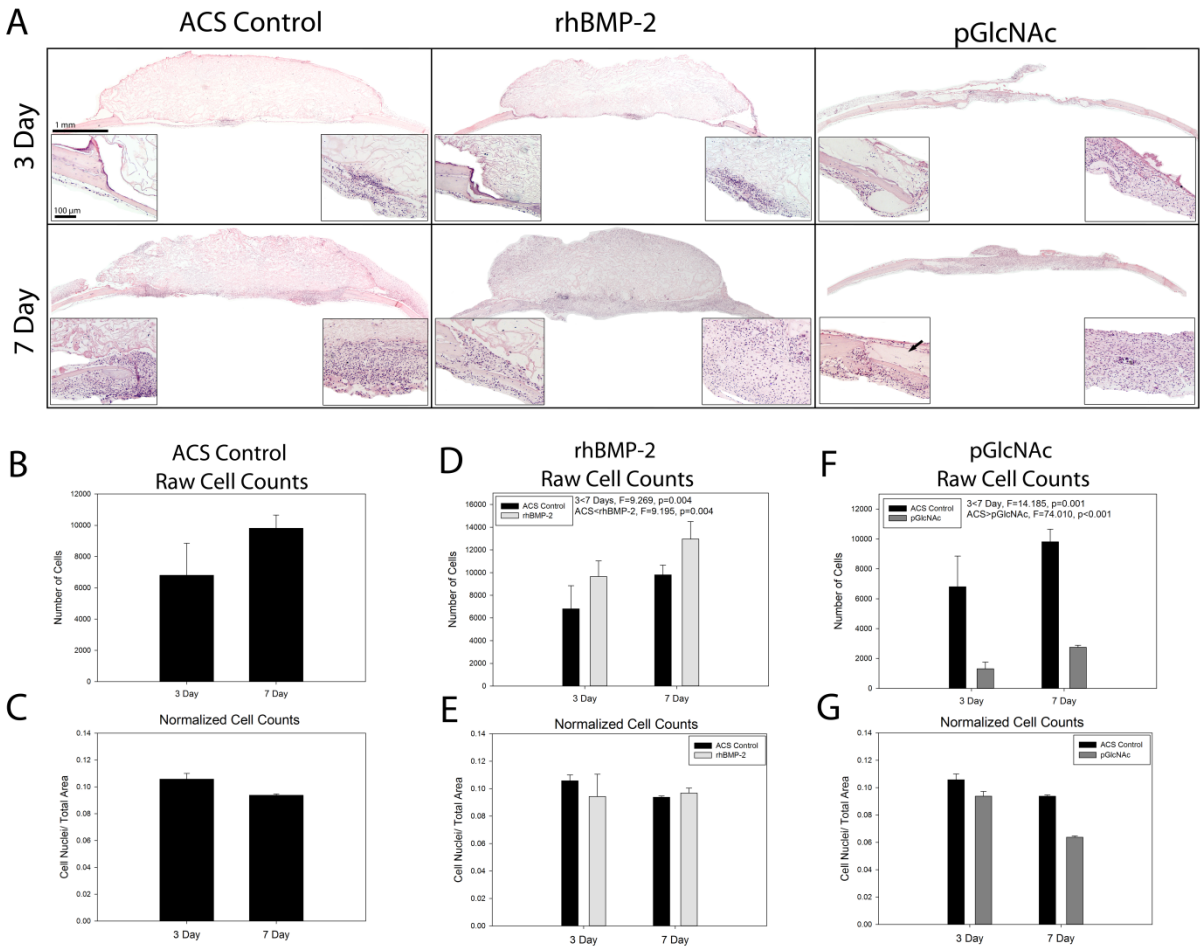

Figure 5. *Hematoxylin and eosin stained calvarial defect section characterization*. **A)** Representative hematoxylin and eosin stained defect sections containing ACS alone, ACS and rhBMP-2, or pGlcNAc. 20x margins (left) and center (right). Increases in cellular infiltrate were noted from three to seven days. Additionally, rhBMP-2 administration resulted in noticeably cellular infiltrate at the margins and ectocranially. The addition of a pGlcNAc nanofiber scaffold to the defect region resulted in the tight compaction of the cellular infiltrate with noticeably more cells at seven days. Further, large areas of space were noted in the pGlcNAc group by seven days (black arrow) **B)** Quantification of nuclei from three to seven days revealed at 42% increase in cellular infiltrate. **C)** When normalized to total volume, analysis indicated there was no difference. **D)** Nuclei counts with the addition of rhBMP-2 showed significant increase in the rhBMP-2 group compared to ACS alone ($p=0.004$) and a significant increase in the number of cells from three to seven days ($p=0.004$). **E)** Normalization of cell counts with rhBMP-2 showed no difference over controls. **F)** Quantification of pGlcNAc treated infiltrate revealed that, despite the cells being much more compact, over all there were less cells present as compared to the ACS control group. Two-way ANOVAs indicated that there was a significant decrease in the number of cells present by seven days ($p=0.001$) and with pGlcNAc administration ($p<0.001$). **G)** When normalized to total volume, analysis indicated there was no difference in pGlcNAc over ACS.

number of cells that responded between three and seven days (**Figure 5B**). While not statistically significant, this does suggest a biological significance.

The ACS and rhBMP-2 treated specimens at three days showed similar trends to that of the ACS control group. rhBMP-2 administration did appear to result in a slight increase in cellular infiltrate into the scaffold in the ectocranial direction. Furthermore, the cells lying along

the dural border and clustered around the sagittal sinus showed a noticeable increase in abundance when compared with the ACS control group. No new matrix deposition was observed with the addition of rhBMP-2 (**Figure 5A**).

At seven days, rhBMP-2 treatment appeared to have markedly increased cellular abundance, infiltration, and new fibrous matrix deposition. There was an apparent increase in the number of cells along the dura compared with the three day time point. However, compared with the seven day ACS control group, cellular abundance along the dura did not appear to be increased. What was apparent was an increase in cellular infiltration into the center of the ACS compared to both the rhBMP-2 at three days as well as the ACS control at seven days. There were particularly noticeable increases within new fibrous matrix deposition at the surgical margins (**Figure 5A**). With the addition of rhBMP-2, there was a significant difference by time ($F=9.269$, $p=0.004$) and a significant difference by treatment ($F=9.195$, $p=0.004$), with seven days and treatment with rhBMP-2 showing an increase in cellular infiltrate (**Figure 5D)**.

pGlcNAc administration resulted in tight compaction of the cells that infiltrated the surgical defect space (**Figure 7A, top**). While the abundance of cellular infiltrate appeared to be similar to ACS alone, the difference in volume of the two matrices likely limited the space available to spread out within the matrix. Cellular infiltrate was more contiguous with the resident bone compared to groups with ACS. The pGlcNAc nanofiber matrix appeared to stain a deep pink with eosin staining, though it was hard to detect, even at this early time point. Scaffold appeared to have broken down significantly with only a thin line of what was believed to be pGlcNAc remaining.

Observation of pGlcNAc administration at seven days showed histological similarities to the ACS at this timepoint; namely, the addition of an increase in cellular infiltrate. Again, differences in matrix volume resulted in tightly packed cells within the surgical margins that were further stressed by the marked increase of cells by seven days. Cellular infiltrate appeared to surround the bone margins on either side of the defect. Virtually no sign of the pGlcNAc matrix

was present by this one week time point; instead, a thick, fibrous network was tightly packed and surrounding the cells that had filled the area (**Figure 5A**). Density of surrounding cellular infiltrate made it difficult to ascertain where the wound bed was compared to the underlying dura. Cell counts compared to ACS alone indicated that treating the defects with pGlcNAc significantly reduced the number of cells within the defect ($F=14.185$, $p<0.001$) without affecting the previously observed increase in cell number from three to seven days ($F=74.010$, $p<0.001$, **Figure 5F**).

Additionally, present in the pGlcNAc treated groups were de-cellularized areas of an unknown composition that did not take up either hematoxylin or eosin stain (**Figure 5A, black arrow)**. These spaces were present in several samples at the three day time point and were still present by seven days. Cells completely surrounded these areas, but were largely not infiltrating, with only a few interspaced purple stained nuclei. The spaces appeared to have a fibril-like composition, though not taking up eosin dye, as would collagen.

Macrophage Polarization

Pan-Macrophage Immunohistochemistry

Immunohistochemistry (IHC) for F4/80, a pan-macrophage surface marker, revealed relatively little immunoreactivity at the three day time point for the ACS control group. Staining was isolated to the cellularized areas, where very faint positivity was observed primarily at the margin. Interestingly, the majority of the F4/80 positive cells were found beneath the resident bone on either side of the defect, rather than in the defect/regeneration space. By seven days, even fewer F4/80 positive cells were observed in the ACS control group. Staining was diffuse and relatively low throughout the cellularized space. Even though more cells were obviously visible by the hematoxylin counter stain, this did not equate to more F4/80 positive cells. Quantification of the positivity revealed that of the portion of tissue subjected to analysis, less than 6% was immunoreactive (**Figure 6B**). Additionally, it was revealed that there was a decrease in F4/80

positivity occurred between three and seven days but was not found to be statistically significant (F=0.241, p=0.625).

In the rhBMP-2 treated group, it was noted that at the three day time point, there was very little positive staining for F4/80. Surprisingly, there was less staining present in the groups treated with rhBMP-2 than in the ACS control group. Staining patterns were localized to the margins which was similar to the ACS control at this early timepoint. Interestingly, by day seven, a dramatic increase in F4/80 positivity was noted. Though faint, F4/80 positive cells were observed around the margins and at the center of the defect, mostly lying along the dura mater

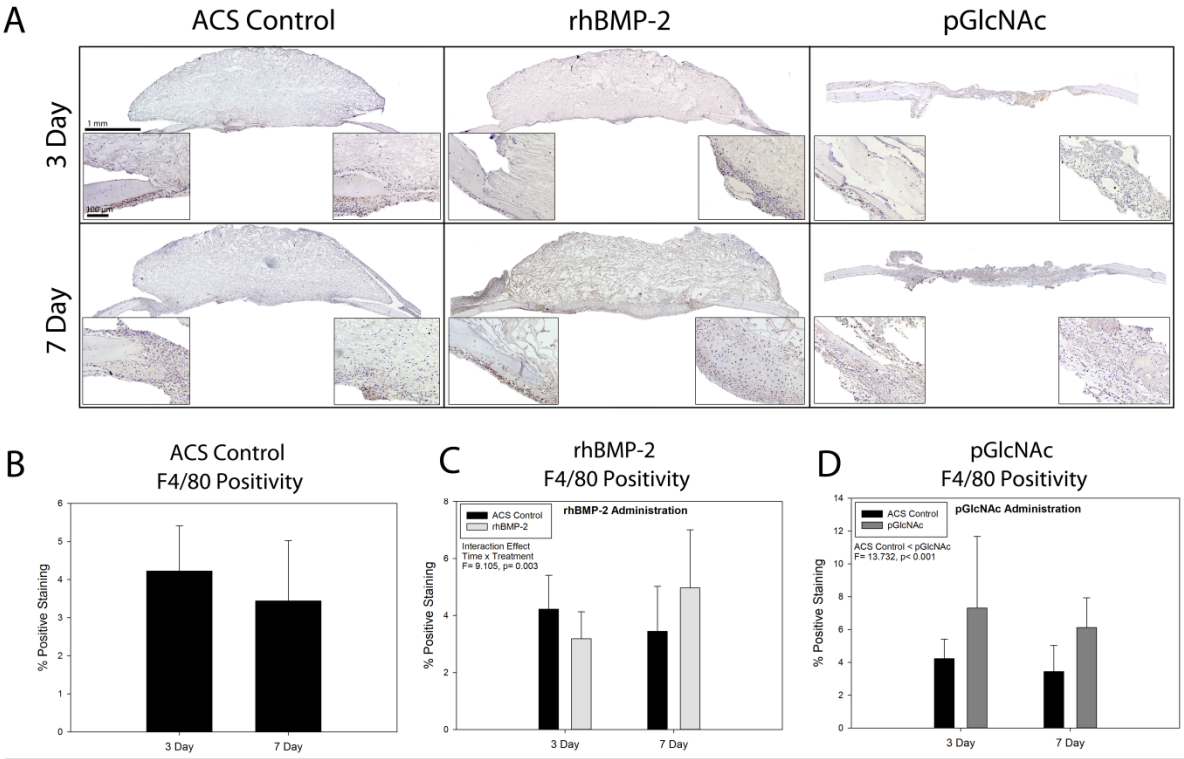

Figure 6. *Characterization of F4/80 expression at three and seven days in ACS, rhBMP-2 and pGlcNAc treated calvarial defects.* **A)** The expression of F4/80 (a pan-macrophage marker) between three and seven days in the ACS control group showed little change. Faint staining for F4/80 was observed with the addition of rhBMP-2. Staining was largely localized to the surgical margins independent of treatment or time point. Percentage of F4/80 positivity appeared to increase with the addition of a pGlcNAc nanofiber scaffold, black arrows indicating area of particularly dense positive staining. **B)** A t-test revealed that there was a slight reduction in F4/80 positivity from three to seven days, though this was not significant (p=0.625). **C)** Quantification and statistical analysis via two-way ANOVA revealed that there was a significant interaction effect with the addition of rhBMP-2 (p=0.003). **D)** Quantification revealed that there was an increase in F4/80 expression with the addition of pGlcNAc at both three and seven days. Two-way ANOVA showed that there was a statistically significant increase in F4/80 expression with the addition of pGlcNAc (p<0.001). 20x margins (left) and center (right).

(**Figure 6A**). In contrast to what was observed in the ACS control group, with rhBMP-2, F4/80 positivity increased significantly from three to seven days. (**Figure 6C**). Statistical analysis revealed that there was a significant interaction effect with rhBMP-2 treatment by time ($F=9.105$, $p=0.003$), where a decrease in F4/80 positive cells occurred early, and then was increased by the seven day time point.

Treatment groups with pGlcNAc scaffold administration showed more F4/80 immunoreactivity at the three day time point than ACS control. F4/80 positivity was more dispersed throughout the defect, rather than being concentrated at the margins (**Figure 6A**). This trend was continued at the seven day time point. Abundant F4/80 positivity was observed in the defect and at the margins at seven days compared to ACS alone. Plaques of densely packed positively stained cells were randomly interspaced throughout the defect. Where cells were tightly packed due to the constraint of the scaffold, tightly packed cellular infiltrate appeared to have F4/80 positivity throughout. There appeared to be denser staining toward the endocranial portion of the infiltrate compared to the ectocranial side. IHC quantification revealed that there was a statistically significant increase in F4/80 positivity at both three and seven days with pGlcNAc treatment (**Figure 6D)** ($F=13.732$, $p<0.001$). Percent positivity was raised to between 6 and 12% of the total area of the analyzed sections. pGlcNAc appeared to significantly increase F4/80 expression at both three and seven days compared to ACS alone.

Polarized Macrophage Immunohistochemistry

Immunohistochemistry for inducible nitric oxide synthase (iNOS) expression (a marker for M1-pro-inflammatory macrophages) in the ACS control group at three days revealed very little positive staining. Where present, staining tended to be juxtaposed to the native bone and were very rarely noticed in the cellular infiltrate. Some positivity was observed on the endocranial side diffusely spread throughout the cells within the dura. By seven days, it was apparent that there was more iNOS positivity present. While the dark, positively stained plaques

were still present at this time point, they appeared to be less common and much smaller when compared to the three day time point. Rather, the cellular infiltrate appeared to show much higher expression of iNOS by seven days. Furthermore, this expression was spread well into the matrix where new cellular infiltrate was observed. iNOS expression was also observed down the length of native bone within canalicular canals of the resident calvarial bone. IHC quantification indicated that there was no significant increase in iNOS expression from three to seven days despite an observed increase in cellular infiltrate and positivity (**Figure 7**).

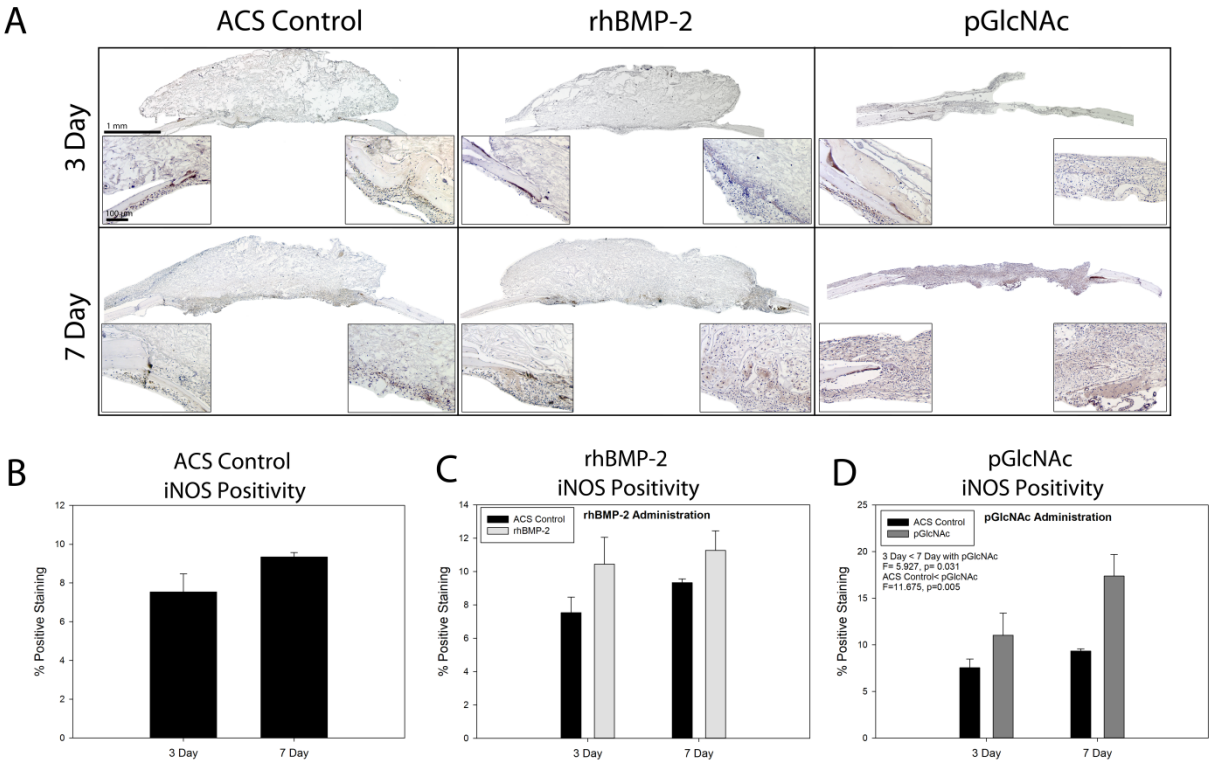

Figure 7. *Characterization of iNOS expression at three and seven days in ACS, rhBMP-2 and pGlcNAc treated calvarial defects.* **A)** Expression of inducible nitric oxide synthase (iNOS), a factor associated with M1-macrophages, was assessed in the calvarial defect via immunohistochemistry. Addition of rhBMP-2 to the defect resulted in slightly more iNOS positive staining when compared to the ACS control. Positivity was localized to the surgical margins within the cellular infiltrate. Addition of pGlcNAc to the defect resulted in a noticeable increase in iNOS positivity. Localization of positivity was found on the endocranial side of native bone as well as in the cellular infiltrate. **B)** Although there appeared to be slightly more iNOS at the seven day time point in the ACS control group, a t-test revealed that there was no significant difference. **C)** Quantification or iNOS positivity in response to rhBMP-2 treatment revealed a slight increase with treatment. Two-way ANOVA was preformed to analyze differences by time and treatment and revealed no difference in iNOS presence with the addition of rhBMP-2. **D)** The Quantification and statistical analysis via two-way ANOVA found that there was a significant increase in iNOS expression from three to seven days with pGlcNAc administration ($p=0.031$) and that pGlcNAc administration resulted in a significant increase in iNOS production compared to ACS alone ($p=0.005$). 20x margins (left) and center (right).

In the rhBMP-2 treated groups, similar expression patterns to those observed in the control group were noted at three days. However, expression of iNOS with rhBMP-2 treatment was more abundant. Aggregates of positivity were observed lining the native bone and surrounding the surgical margins. Cells lining the dura also showed positivity for iNOS expression, though this was very faint. Lack of cellular infiltrate into the matrix meant that very little iNOS expression was observed in the scaffold of the rhBMP-2 treated group at this time point. At seven days, there was little change observed in the overall abundance of iNOS expression with rhBMP-2 treatment. As with the ACS control group, a shift in expression pattern

was observed where the dense plaques of positive staining turned to more diffuse staining within the cellular infiltrate. Staining in this case did appear to be concentrated at the surgical margins but was also found in the canals of the native bone (**Figure 7A**). Quantification revealed that rhBMP-2 treatment did increase iNOS expression slightly when compared to control, however, this was not statistically significant upon analysis (**Figure 7c**, F=4.355, p=0.059).

Administration of pGlcNAc to the calvarial defect proved to have a dramatic effect on expression of iNOS at three and seven days compared to ACS alone (**Figure 7A**). At the three day time point, cells that were in and surrounding the defect area showed more regularly spaced iNOS positivity. This was particularly noticeable in the cells that were underlying and infiltrating the native bone, which showed dark expression of iNOS in close association with nuclei. It was also noticed that the plaques of unknown composition that were noted in the hematoxylin and eosin analysis were lightly immunoreactive to iNOS IHC. This is evident at the three and seven day time points. A marked increase in positivity was noticed by seven days. As with the rhBMP-2 treatment, the increase in cellular infiltrate was complimented by an increase in iNOS expression. Additionally, darkly stained plaques of positivity remained present at seven days with the addition of pGlcNAc. Quantification of the IHC supported this observation, indicating that iNOS expression was significantly elevated in response to pGlcNAc administration (**Figure 7D**). Furthermore, more iNOS positivity was present at seven days than at three days with this treatment. Statistical analysis revealed that both of these observations were significant; iNOS positivity with pGlcNAc treatment was greater than in ACS alone (F=11.675, p=0.005) and more iNOS expression was present at seven days than at three with pGlcNAc treatment (F=5.927, p=0.031).

Immunohistochemistry for arginase-1 (Arg1), an important enzyme involved in collagen synthesis and indicative of M2-pro-reparative macrophages, in the ACS control group showed light, diffuse staining throughout. Where cell presence was noted, there were normally also Arg1 positive cells. At the three day time point, positivity was reserved primarily to the cells within the

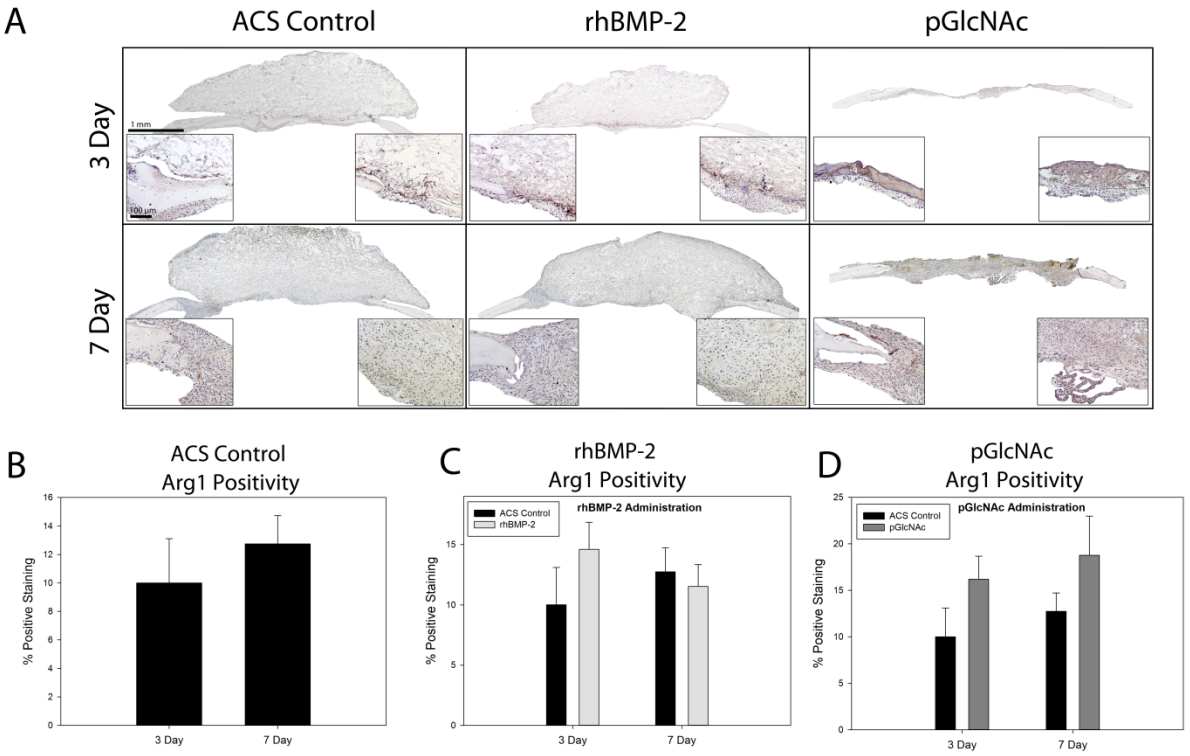

Figure 8. *Characterization of Arg1 expression at three and seven days in ACS, rhBMP-2 and pGlcNAc treated calvarial defects*. **A)** Immunohistochemistry for arginase-1 (Arg1) expression, a factor associated with collagen synthesis and M2 reparative macrophages, was performed on three and seven day samples. Addition of rhBMP-2 to the defect resulted in an increase in Arg1 positivity, particularly noticeable at the three day time point. Positivity was spread throughout the infiltrate area as well as localized at the surgical margin. Administration of a pGlcNAc nanofiber scaffold resulted in an increase of Arg1 positivity in the defect area that was apparent at both three and seven days **B)** A t-test revealed that there was no significant increase in Arg1 expression between three and seven days. **C)** Quantification revealed that overall there was no significant difference in Arg1 expression by time or treatment with addition of rhBMP-2, as assessed by two-way ANOVA. **D)** Despite the observed increase in Arg1 positivity following pGlcNAc treatment, a two-way ANOVA indicated that there was no significant difference between time or treatment ($p=0.062$). 20x margins (left) and center (right).

dura as well as the native bone. This expression pattern was maintained out to the seven day time point. Staining for Arg1 remained relatively diffuse, even in the presence of increased cellular infiltrate. Quantification of the positivity indicated that Arg1 expression remained similar from three to seven days in the ACS control group, with only a slight, insignificant increase by seven days (**Figure 8**). Additionally, it was noted that Arg1 expression and percent positivity of the analyzed sections were comparable to that of iNOS.

The addition of rhBMP-2 to the scaffold resulted in what appeared to be increased Arg1 staining at the three day time point. Arg1 positivity was localized along the cellular infiltrate just

above the dura. Interestingly, there was a clear division in the expression pattern at three days, with cells that were positive for Arg1 beside similar cell-types that were negative for Arg1 (**Figure 8A**). Arg1 staining remained largely in the endocranial side of the scaffold, as with the previous stains. By seven days, Arg1 positive staining appeared to have decreased in the rhBMP-2 treated samples. Staining was much more diffuse than what was observed at three days. Despite the apparent increase in cellular infiltrate, there was no increase in Arg1 positive cells. Light staining was visible throughout the infiltrate and in close proximity with nuclei. Quantification showed that there was a slight decrease in Arg1 expression from three to seven days with rhBMP-2 administration (**Figure 8C**). However, statistical analysis did not reveal a significant difference. Additionally, there was not a significant difference observed between treatments, indicating that Arg1 expression remained consistent to the ACS alone group with the additional rhBMP-2.

The administration of a pGlcNAc nanofiber scaffold in the defect had little impact on Arg1 expression. pGlcNAc treatment did not seem to concentrate the Arg1 positive cells to a specific area, as was observed with rhBMP-2 treatment at three days. Rather, expression was diffuse and relatively uniform throughout the infiltrate. Arg1 positivity was noticeably higher than ACS control at this time point. Further, cells positive for Arg1 were closely associated with the resident bone and surrounding the surgical margin. By seven days, cellular infiltrate had increased with pGlcNAc administration but little difference in the abundance of positive cells was noted. As the pGlcNAc scaffold was thinner and thus resulted in more compact infiltrate, it was noticed that there was a defined line between where the Arg1 positive cells and Arg1 negative cells of the matrix existed at the seven-day time point (**Figure 8A**). Aggregates of Arg1 positive staining where noted as well in the defect; however, these did not appear to be the same aggregates of unknown composition noted in the H & E's. Arg1 expression was not closely associated with cell nuclei, but rather the fibrous matrix that surrounded the cells. Quantification revealed that there was a slight increase in Arg1 expression with pGlcNAc administration over the ACS control (**Figure 8D)**, but statistical analysis revealed that it was not significant (F=4.237,

p=0.062). Furthermore, there appeared to be a slight increase in Arg1 expression between three and seven days, though statistical analysis confirmed that it was not statistically significant.

As macrophage polarization is often not clearly defined *in vivo* and exists within a spectrum, the ratio of markers for M1 and M2-macrophages is more informative of getting a broad spectrum appreciation of macrophage phenotype with in the healing defect. As this was a calculation based on M2-macrophages to M1-macrophages, a larger number would be indicative of a more reparative phenotype. There was no significant difference in the ratio of Arg1:iNOS between three and seven days in the ACS control group (**Figure 9A**).

When comparing the ratio of arginase-1 (Arg1) expression to inducible nitric oxide synthase expression (iNOS) in order to investigate the nature of the inflammatory response and the polarization of macrophages, rhBMP-2 did not appear to drive macrophage polarization in any particular direction (**Figure 9B**). Interestingly, rhBMP-2 administration slightly increased the M2-phenotype ratio at the three day time point while slightly decreasing this phenotype by seven days. Despite the apparent changes, statistical analysis revealed that there was no significant difference in Arg1:iNOS ratios with rhBMP-2 treatment.

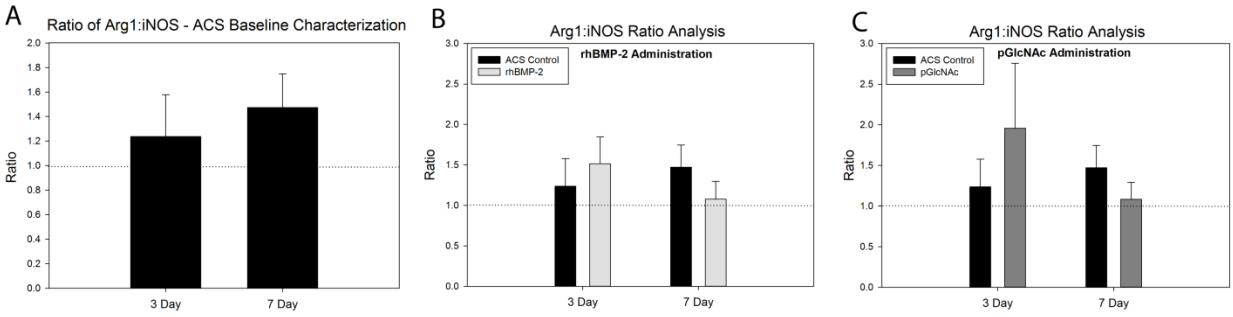

Figure 9. *Ratio of Arg1:iNOS following the administration of rhBMP-2 and pGlcNAc at three and seven days.* The ratio of Arg1:iNOS was calculated to determine if a particular macrophage phenotype was preferred between three and seven days. A larger ratio indicates a more reparative (M2) phenotype. **A)** There appeared to be more M2-like response present by seven days, though a t-test indicated that this increase was not significant. Dotted line represents 1:1 net neutral macrophage phenotype. **B)** The addition of rhBMP-2 to the defect area resulted in little changes to the overall macrophage polarization. **C)** Addition of pGlcNAc resulted in a slight increase in an M2-like phenotype that resolved by seven days. Two-way ANOVAs indicated that there were no significant differences between the M2/M1 ratio. Dotted line represents a 1:1 net nuetral macrophagbe phenotype.

A similar trend was noted when performing the ratio analysis for pGlcNAc administration. The addition of pGlcNAc resulted in a marked increase in the Arg1:iNOS ratio compared to the ACS control at three days. Furthermore, the addition of pGlcNAc to the defect resulted in a decrease in the ratio of Arg1:iNOS at seven days. Again, though there were observational differences in the ratio of Arg1:iNOS with treatment and with time, statistical analysis did not reveal significant differences with pGlcNAc administration (**Figure 9C)**.

Inflammatory Cytokine Western Blot Analysis

Cytokines selected based on a previously performed inflammatory protein array and indicated in the literature as being important in bone wound healing were analyzed by western blot analysis to confirm results obtained from the array. Initially, the western blot for TNF-α performed with three and seven day samples did not show bands at the predicted 26 kDa (immature/preprocessing) molecular weight or the 17 kDa (secreted) molecular weight level. It was determined that cytokine array data suggested that the concentration of these targets (specifically TNF-α in this case) was in a low abundance, ~1 pg/mL to ~350 pg/mL. Running a western blot for recombinant mouse TNF-α revealed bands at 17 kDa; however, serial dilutions of the TNF-α recombinant showed that, with our detections system, bands were only detectable down to about the 1000 ng/mL concentration. This was nearly five logs higher than what was found by the array. Western blots for recombinant mouse MCP-1 and recombinant mouse IL-17 revealed that bands could be detected at the 100 ng/mL and 1000 ng/mL concentrations, respectively. Thus, it was determined that these targets were outside of the limit of detection for our western blot system due to their low abundance in the extracted healing bone tissue (**Appendix,** Supplemental Figures 1, 2, and 3).

Angiogenesis

VEGF Western Blot Analysis

Western blots performed on protein isolated from the three and seven day regenerate in the mouse calvarial critical sized defect (CSD) revealed a detectable band at the predicted 43 kDa for VEGF-A. Analysis of the blot revealed that treatment with rhBMP-2 and pGlcNAc resulted in changes to band intensity (**Figure 10A, arrow pointing to VEGF**). Though previous cytokine array data from our lab indicated that rhBMP-2 administration resulted in a statistically significant increase in VEGF expression at three days, the western blot did not support this. Instead, western blot analysis suggested that there was a decrease in VEGF expression with rhBMP-2 administration at three days. Seven day cytokine array data also indicated that VEGF expression was reduced at seven days compared to ACS control. VEGF expression was not noticeably reduced compared to ACS control at seven days with the administration of rhBMP-2. Administration of pGlcNAc resulted in a decrease in VEGF expression at three days when compared in the ACS control group. This reduction in VEGF was continued out to seven days, unlike with rhBMP-2 administration.

Normalizing protein concentrations to total protein loaded and quantifying the band intensity based on three separate gels revealed that there was a slight increase in VEGF expression by seven days, though this was not significant (**Figure 10B**). The administration of rhBMP-2 did in fact result in a decrease in VEGF expression at three days compared to ACS alone. However, VEGF expression with rhBMP-2 administration at seven days showed similar levels to control (**Figure 10C**). Administration of pGlcNAc lowered VEGF expression at three

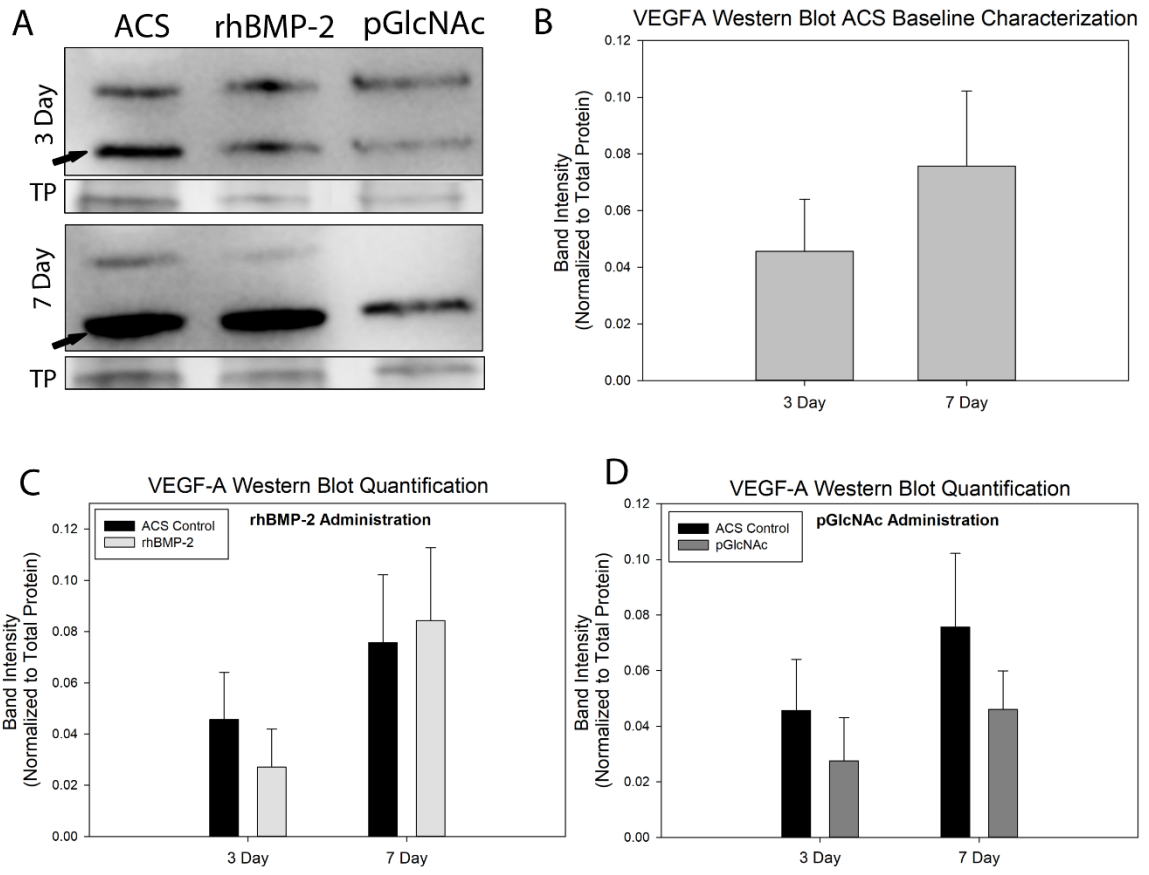

Figure 10. *Expression of VEGF-A in protein samples collected from CSD regenerate.* Western blots for VEGF-A were performed for three and seven day samples from animals in the ACS control, ACS rhBMP-2, and pGlcNAc groups (A). A band was detected by the VEGF antibody at 43 kDa, as expected (black arrows). Additionally, an aberrant band was detected at around 50 kDa (top band). Total protein (TP) was used a loading control for downstream analysis. Quantification of band intensity normalized to total protein loaded was performed for the ACS control group at three and seven days (B) as well as for the groups treated with rhBMP-2 (C) and pGlcNAc (D). Statistical analysis revealed that there was no difference between three and seven days for the control group. Additionally, two-way ANOVAs for differences in the treated groups compared to control did not reveal any significant differences.

days and seven days (**Figure 10D**). Despite the modulation of VEGF expression in defect regenerate, statistical analysis performed on the quantified band intensities did not yield any statistically significant differences by treatment compared to control or by time.

Identified in the blots was another band at approximately 50 kDa that also appeared to respond to treatment and that was tagged by the VEGF antibody (**Figure 10A, top band**). This band appeared to have a similar intensity to that of the identified VEGF bands at three days. By seven days, however, the intensity of this upper band had faded dramatically in all of the groups; but particularly in the treated rhBMP-2 and pGlcNAc groups. With pGlcNAc administration at seven days, there was no 50 kDa band detectable at all. As these bands were not identified at the predicted molecular mass of VEGF, they were not quantified.

PECAM Immunohistochemistry

Immunohistochemistry for platelet endothelial cell adhesion molecule (PECAM), a marker of vessel presence, was performed to determine if differences in VEGF expression were leading to angiogenesis and ultimately healing (**Figure 11A**). While vessel formation was able to be visualized via IHC for PECAM, vessels that were observed appeared to be mature and residing in the dura mater or sagittal sinus. These vessels were large comparatively and likely not representative of new vessel formation that would be indicative of healing. Vessels were stained brown on the interior of the vessel wall (endothelial cells). There were unstained cells surrounding vessels. Presence of these vessels was sparse throughout the entire selection of specimens. In addition to obvious vessels, PECAM positivity was also observed throughout the defect. Analysis of PECAM positivity was performed both for the whole defect as well as for specific regions believed to be important for healing. A regional analysis of PECAM positivity was used to determine where PECAM, and subsequent angiogenesis, may be occurring in the defect. Quantification of these regions of interest provided a graphical interpretation of where PECAM was in the sample based on percent positivity of the region of interest. Three unique

regions of interest were chosen (sinus related, non-sinus related, and surgical margin, defined in **Figure 4**).

In the ACS control group, PECAM positivity was noted around the surgical margins and

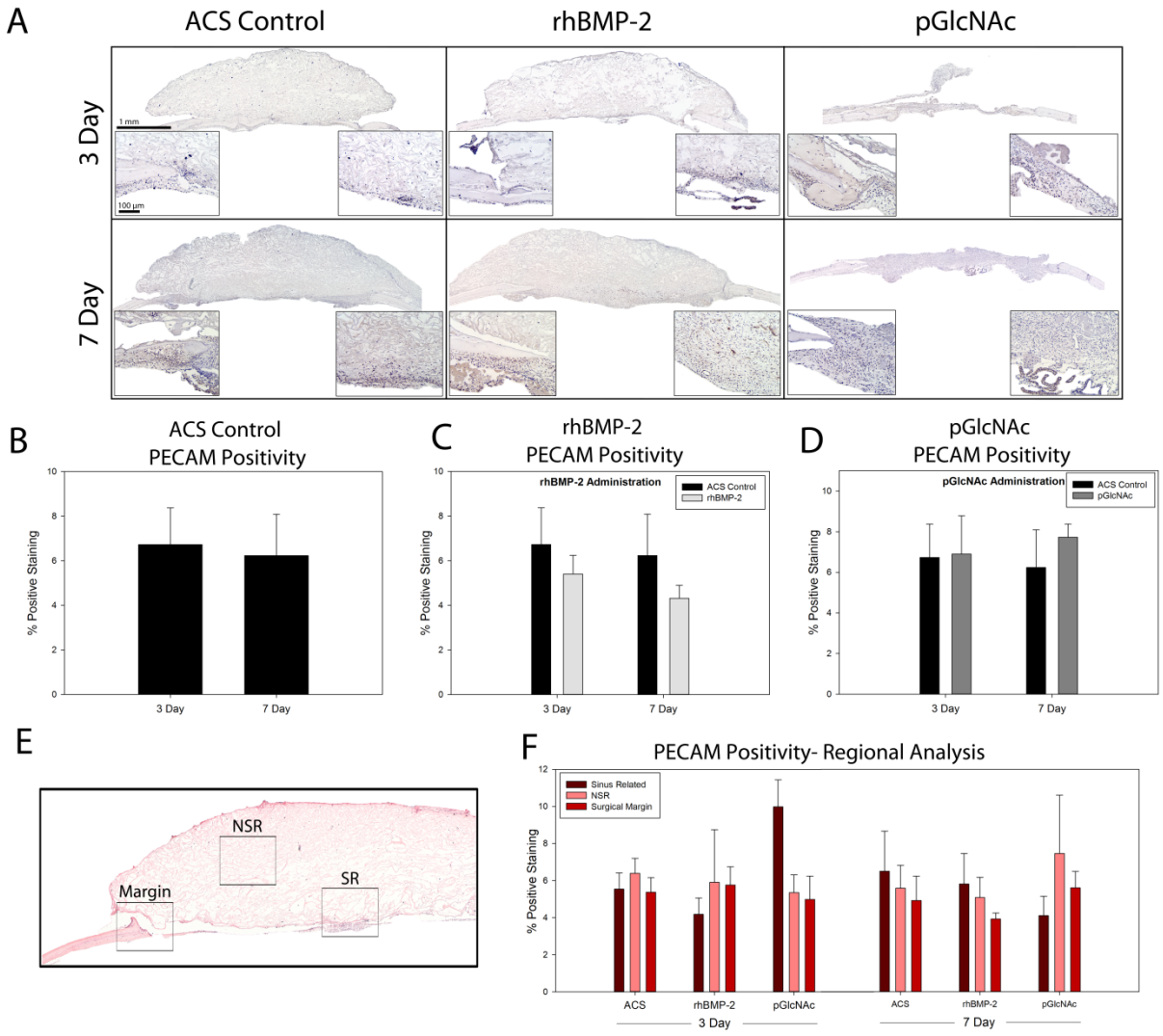

Figure 11. *Characterization of PECAM expression at three and seven days in ACS, rhBMP-2 and pGlcNAc treated calvarial defects.* **A)** IHC for PECAM expression revealed that very little vasculature was present in the regenerated tissue at either time point or with any treatment. Positive vasculature was localized to resident vessels in the underlying dura. **B)** Baseline characterization of PECAM expression indicated that there was no difference in PECAM expression between three and seven days. **C)** Quantification and statistical analysis via two-way ANOVA indicated that there were no differences with rhBMP-2 treatment. **D)** Quantification of PECAM and subsequent two-way ANOVA revealed that there was no difference in PECAM expression following pGlcNAc adminsitration. **E)** Specific regions of known importance in healing were analyzed for sub-localization of PECAM positivity (Margin= surgical margin; SR= sinus related; NSR= non-sinus related). **F)** A three-way ANOVA indicated that there were no significant differences in regional PECAM locality by time or treatment. 20x margins (left) and center (right).

in conjunction with cells at three days. Staining was also noted within the dura, particularly on the endocranial side of the infiltrate. By seven days, staining patterns remained relatively unchanged. Staining appeared to be slightly darker and more concentrated at areas of substantial cellular infiltrate, but only marginally higher than that of the three day time point. Quantification and statistical analysis of the ACS control indicated that there was no change in PECAM expression between three and seven days (**Figure 11B**). Regional assessment of PECAM localization from three to seven days, the ACS control group did not appear to have any sub-localization of PECAM in the wound bed (**Figure E,F**).

The addition of rhBMP-2 resulted in a slight decrease in PECAM expression at three days. Staining patterns were consistent with the ACS control group at this time point with less positivity (**Figure 11A**). Despite there being more cells present with rhBMP-2 administration, this did not equate with more PECAM expression and subsequent angiogenesis. This remained consistent at seven days as well. rhBMP-2 administration at seven days led to a slight decrease in PECAM expression when compared to both the ACS control group, as well as, the three day rhBMP-2 group. PECAM positivity was less ubiquitous and isolated primarily to the surgical margins and sinus area at seven days. Quantification of PECAM positivity revealed that rhBMP-2 reduced overall expression of PECAM compared to the ACS control. Further, PECAM expression was decreased at seven days when compared to the three day time point (**Figure 11C**). Statistical analysis showed that there was no statistical difference in PECAM positivity between the rhBMP-2 treated groups and the ACS control groups. The administration of rhBMP-2 slightly decreased the contribution of sagittal sinus related PECAM positivity compared to the control (**Figure 11F**). The surgical margin and the non-sinus related (NSR) sections of defect had similar levels of positivity to each other and to the ACS control group at three days.

Staining for PECAM in defects implanted with the pGlcNAc scaffold showed staining patterns and abundance that was very similar to the ACS control group. At three days, staining for PECAM was present at the surgical margins primarily but also found throughout the defect space.

Due to the thin nature of pGlcNAc, staining was not concentrated endo- or ecto-cranially (**Figure 22A**). It should be noted that the unknown substances found in the H&E samples stained lightly positive for PECAM. By seven days, with the increase in cells there was also a slight increase in PECAM abundance. PECAM positivity was apparent throughout the defect as with the three day time point. Quantification revealed that PECAM positivity was slightly higher than ACS control with pGlcNAc treatment at both three and seven days, though statistical analysis did not show any significant differences (**Figure 11D**). In samples that were treated with pGlcNAc scaffolds, the sinus related PECAM positivity was up much higher than in the control ACS or rhBMP-2 treated groups. Similar to the ACS and rhBMP-2 groups, the surgical margin and NSR space contributed similar amounts of PECAM (**Figure 11F**). Statistical analysis of the regional defect PECAM abundance revealed that there was no significant difference in PECAM by region.

Overall, PECAM levels were relatively similar at three days as at seven Seven day ACS control regional analysis showed that there was slightly more contribution to PECAM abundance in the sinus related areas. This was followed by the NSR area. Though only slightly lower, quantification indicated that the surgical margin contributed the least to PECAM abundance in the seven day ACS control group. Nearly the exact same trend was observed with the rhBMP-2 treated group at seven days. Sinus related areas of the defected contained more PECAM positivity than non-sinus related areas, which contained more PECAM positivity than the surgical margin. While the trend across the board indicated that the sinus related areas contributed the most to PECAM abundance; pGlcNAc treated groups were the exception to this observation in that they appeared to have the lowest sinus related contribution, particularly in the seven day cohort. Interestingly, with pGlcNAc administration, there was a marked increase in NSR related PECAM positivity. Contribution of the surgical margin was higher compared to the rhBMP-2 treated group with pGlcNAc administration but overall consistent with other observations of the surgical margin. Statistical analysis did not indicate that there were any differences in specific regions as it deals with PECAM abundance and localization. Furthermore, statistical tests between three and

seven days matched with data obtained in the whole defect quantification and indicated that there were no differences in PECAM positivity within specific regions between three and seven days.

CHAPTER 6

Discussion

Summary of Results

In an effort to determine whether heightened inflammation contributed to failure associated with INFUSE® (ACS loaded with rhBMP-2) and if inflammation could be altered to lead to better healing outcomes, this present study characterized baseline inflammatory response as associated with ACS alone. It was found that there were no statistically significant differences in cellular infiltrate from three to seven days, despite an apparent 42% increase in the number of cells by seven days. Additionally, there were no significant changes in total macrophages present nor markers associated with a downstream M1/M2 polarization phenotype. Finally, the levels of markers associated with angiogenesis remained largely unchanged.

The addition of a subclinical dose of rhBMP-2 did not result in a significantly robust inflammatory response. While rhBMP-2 did increase cellular infiltrate, there were no signs of caustic damage occurring. Macrophages, positive for F4/80 were not changed dramatically either, though rhBMP-2 may result in a delay of macrophage response. Arguably more important, is that rhBMP-2 delivery did not polarize macrophages to an early M1 response. In fact, it was apparent that there was no specific polarization occurring in response to rhBMP-2 delivery. There was no increase in VEGF-A production associated with rhBMP-2 delivery nor were there any changes in PECAM expression patterns with this therapeutic.

Using a pGlcNAc nanofiber scaffold in a critical sized defect significantly decreased the number of cells infiltrating the wound site when compared to the ACS alone; likely leading to decreased healing as well as signaling. Compaction of cellular infiltrate was, however, noticeably higher than in the ACS group. Additionally, pGlcNAc treatment led to a significant increase in the number of macrophages in the defect area, evidenced by an increase in F4/80 positivity. Additionally, there was a significant increase in iNOS, a marker of pro-inflammatory macrophage

activity; despite this increase, there was no correlation to a more M1-like phenotype downstream. pGlcNAc administration appeared to negatively affect VEGF expression overall but had no effect on PECAM levels.

Overall, inflammatory modulation appeared to be only marginally altered by these therapies compared to the baseline, with the majority of analysis indicating that there were no biologically significant changes. Many of the changes observed did not prove to be significant statistically and many of the statistically significant differences resolved to normal levels by the later time point. Thus, it can be concluded that rhBMP-2 delivery at this dose does not increase baseline ACS induced inflammation and nor is it lowered by treating the critical sized defect with an anti-inflammatory pGlcNAc nanofiber scaffold.

Extrapolation of Data

The use of rhBMP-2 as a therapeutic modality has revolutionized the field of bone tissue engineering[39,42,43,45,48]. Despite its wide-spread use and successes, adverse side effects associated with the use of rhBMP-2 has led to questions about the efficacy and safety of this product. Often cited with the use of rhBMP-2 is rampant and/or prolonged inflammation, among other detrimental side effects[12,13,42,46,51,52]. Still, very little research has been done to confirm and investigate the pathway of effects of these clinical observations following treatment.

This present study aimed to provide a baseline characterization of the rhBMP-2 commercially provided carrier, *acellular collagen sponge* (ACS). The current body of literature suggests that there are defined steps through which modulation of inflammation occurs following a fracture, particularly in the early, acute phase[1,2,14,16,28,31-33,35,40,68,69]. However, the lack of change in macrophages and angiogenesis from three to seven days in our baseline characterization suggest that ACS itself may be affecting inflammation, potentially through several mechanisms. For instance, as ACS is comprised entirely of collagen, it is believed to be relatively inert in the healing environment. However, at least one study has pointed out that the administration of ACS alone caused local inflammation and as a result the addition of rhBMP-2 does not necessarily

increase this inflammatory response[18]. It could be that adding ACS to the bony defect simply masks the effects of any modulation we may see. Alternatively, ACS may provide a mechanism through which inflammation is sustained through the healing process, rather than being resolved as the transition into the healing phenotype occurs. This is still an area of ongoing research in the field. One hypothesis could be that ACS promotes a prolonged foreign body response as the large scaffold is remodeled into matrix. Thus, inflammation would be sustained over time and minute alterations in inflammation would be difficult to detect.

This study further aimed to evaluate how the inflammatory responses were altered by the addition of rhBMP-2 or with a pGlcNAc nanofiber scaffold used to augment healing in skin wounds. Our hypothesis was that the addition of rhBMP-2 would result in noticeable changes to the inflammatory response necessary for bone wound healing, marked by altered inflammatory cytokine levels, classical M1 activation of macrophages, and decreased healing and angiogenesis. Additionally, based on the ability of pGlcNAc nanofiber scaffolds to reduce inflammation in cutaneous wounds and provide for better healing outcomes, we hypothesized that treating a calvarial defect with pGlcNAc would result in an earlier M2-macrophage polarization and increased angiogenesis. Contrary to what was expected, delivery of this subclinical dose of rhBMP-2 did not appear to dramatically affect macrophage populations or angiogenesis. Furthermore, there were almost no signs that the addition of rhBMP-2 led to a heightened inflammatory response. It is also clear that pGlcNAc did not have an extraordinarily noticeable effect on macrophage populations, or angiogenesis.

The lower cell counts and lack of anti-inflammatory cell response with pGlcNAc administration may be due to the difference in thickness between the pGlcNAc scaffold and ACS. Noticeably lower cell counts were observed with pGlcNAc treatment. This could be due to a simple difference in volume. Furthermore, overcrowding of the defect region could have resulted in competition for resources and apoptosis through cell-to-cell contact. This could account for why pGlcNAc did not modulate inflammation. Another key difference could be found in the type

of cells that respond in these different tissue injuries. Healing is very similar between bone and skin, however, different cells do respond. Perhaps migrating and proliferating keratinocytes more readily respond and adhere to pGlcNAc than do osteoblasts and osteoclasts. Additionally, inflammatory signaling pathways that are activated may be cell type specific, and thus, pGlcNAc may signal differently through these different cells. Much more research is necessary to better understand how pGlcNAc is modulating inflammation from cell niche to cell niche.

Though these treatments both appeared to have a significant effect on F4/80 expression (macrophage populations), it is important to note that staining was relatively low in all groups and treatments. This suggests that these treatments may be having little effect on macrophage activation and migration. While the scaffolds did allow for a substantial amount of cellular infiltrate, it appears that these cells were not macrophages. Additionally, staining for the M1/M2 macrophages was light, indicating that the macrophages that were present were not polarized towards one direction or the other. The lack of immunoreactivity present in the defect areas is likely reflective of a lack of macrophages present in the regenerate at all.

An interesting observation was made in some of the staining patterns for iNOS specifically. It known that NO is important for bone formation and maintenance as a whole, and so, its presence in resident bone would be expected.[40] However, positive iNOS staining was observed within canals of the resident bone, in what appear to be Havarsian canals of osteons. This is somewhat surprising. Literature suggests that the adult mouse bone does not undergo osteonal remolding as humans do[70]. The fact that calvarial bone in mouse has been poorly characterized could give some explanation as to this observation. It is possible that the calvaria of these eight week old mice may undergo osteonal remodeling that is not seen elsewhere in the body.

It was hypothesized that the abnormal edema associated with rhBMP-2, along with seroma formation, may be in part due to an increased angiogenic potential as a result of growth factor delivery. As rhBMP-2 is a growth factor, part of the TGF-ß family, it was expected that

this treatment would result in an increase in other growth factors, especially those associated with angiogenesis and healing (i.e. VEGF)[16,42,69,71]. Additionally, cytokine array data from our lab indicated that rhBMP-2 results in an early increase in VEGF expression which resolved by seven days **(Appendix,** supplemental Figure 4**)**. The opposite appeared to be true based on abstracted western blot data.

While the reason for the differences between the western data and the cytokine array data are unknown, it is important to acknowledge the differences in the assays used to acquire these data. The cytokine protein array is essentially an enzyme linked immunosorbent assay (ELISA), which is much more sensitive than a western blot, but less specific. I could be that the array data is reflective of proteins that are other varients of VEGF, not specifically VEGF-A, as was assayed by western blot. Further, it is possible that the band observed at 50 kDa is a post-translationally modified version of VEGF-A. This band did appear to respond to treatment similar to VEGF-A. As it was not used in the quantification due to not being at the level suggested for VEGF-A, this band may be a variant of VEGF. It is well known that the VEGF-A receptor (VEGFR-2) is post-translationally modified and that this leads to alterations in signal transduction.[72] As the VEGF receptor is much larger than VEGF-A (>200 kDa) it is unlikely that this band is receptor bound. It is also known that different isoforms of VEGF-A mRNA exists through alternative splicing.[73] Post-translationally, VEGF-A can also be modified in response to different cellular processes.[74] The most likely explanation for this band is an alternative isoform of VEGF-A or a shorter section as a result of degradation during processing.

PECAM levels remained unchanged with rhBMP-2 treatment. This may be due to seven days being too early of a time point to capture new vessel formation in our model. Thus, it cannot be definitively said that angiogenesis and subsequent leaking fluid would lead to the observed clinical outcomes following rhBMP-2 administration.

Limitations

Concerning rhBMP-2, it is important to emphasize that the dose used in this study was subclinical. The reason for this is based on previous data collected from our group (recently submitted for publication). A previous arm of this study was aimed at investigating definitive healing outcomes with the administration of rhBMP-2 and pGlcNAc at four and eight weeks. Data from that study indicated that the 325 ng dose of rhBMP-2, used here and representing our "medium" dose, provided the best preclinical healing outcomes (data recently submitted for publication). Thus, this dose was selected for these inflammation experiments to better understand the interaction between inflammatory modulation and healing.

The dosing schema used in our experiments could at least partially account for the lack of aberrant inflammation. Bone morphogenetic proteins, including BMP-2, are found endogenously, but at levels much lower than what is administered in the scaled murine clinical dose (5 μg). BMPs act in a positive feedback loop, with BMP-2 initiating more production of BMP-2 and so on. Supraphysiological levels of BMP-2 could be over stimulating this cascade, leading to activation of inflammatory pathways and subsequent signaling leading to the abnormal activation of inflammatory cells. Further, our lab has shown that as much as 40% of rhBMP-2 loaded on to the ACS scaffold is released (leach out) and dissipates from the healing site in under an hour **(supplemental Figure 5)**. This rapid release of growth factor likely leads to over stimulation of cells (i.e. resident bone cells, surrounding myocytes and adipocytes, chondrocytes, etc.) found in the surrounding tissue that would normally not be involved in the healing process. By reducing the dose, the concentration of released growth factor is likely proportionately reduced. Therefore, dose may be a contributing factor to the lack of inflammation observed in this study. Thus, a lower dose of rhBMP-2 may lead to better clinical application.

An additional limitation can be found in the lack of a full understanding of the mechanism by which pGlcNAc nanofibers reduce inflammation in skin and result in better healing outcomes. Preliminary data has shown that pGlcNAc nanofibers can modulate

inflammation through TLR4 in an NF-kB independent manner, albeit in a cutaneous wound (data unpublished). There was no indication that pGlcNAc was able to modulate inflammation in bone wounds via the methods we chose. While healing is similar in most tissues, the unique cells found in bone may not have the appropriate factors necessary to respond to this treatment as cutaneous cell types. Due to the action of pGlcNAc on collagens in the skin and its regeneration without scarring, it was hypothesized that this biomaterial may have a similar effect on the collagen in bone and result in better healing outcomes along with the noted anti-microbial and anti-inflammatory effects. This, however, did not prove to be true. It could be that the mechanism of action for reducing inflammation is not mediated by macrophages and, thus, would not result in a phenotypic shift. Additionally, as the cells that respond to skin wounds are different from the cells responding to bone wounds, pGlcNAc may not activate these cell niches in the same manner. A finally point could be made that there was not sufficient challenge to the wound site, resulting in little inflammation to begin with.

A different feature that needs to be addressed is our surgical model, the murine calvarial critical sized defect. One of the major strengths of this model is the rapidity and standardization of usage that allows for high through-put, minimal animal morbidity, and easy downstream quantification; unfortunately, this innate strength may also be a pit-fall for this type of study. By definition, the critical sized defect is one that will not completely regenerate spontaneously during the life of the animal.[63] This is largely due to the lack of signaling from opposite sides of the surgical margins that is necessary for proper healing. This is advantageous in interrogating healing modalities and tissue engineering strategies, but the same signaling that is necessary for proper healing is also critical for the early inflammatory response. Thus, this model may not be the best for allowing propagation of these signaling cascades. Additionally, as surgeries are planned and performed aseptically and apply very little trauma, there may not be sufficient challenge to initiate the appropriate healing cascades[75].

A final limitation may be found in the time points selected for this study. Literature indicates that the initial inflammatory cascade following fracture starts immediately to within 24 hours.[2] As neutrophils respond within 24 hours, they are quickly replaced by M1 macrophages within a few days. These macrophages signal further, resulting in M2 macrophage polarization and recruitment. Through several steps, inflammation starts within a few days and continues to as much as two weeks.[1,2,32] It is true that our preclinical mouse model may not appropriately model what is seen in humans. This is particularly true with bone wound healing; though studies have shown that other types of wound healing can effectively be modeled in a murine model[76]. The early inflammatory response following a bone wound in the mouse model has still yet to be comprehensively characterized. Further investigation into the inflammatory response in the mouse calvarial defect model, as well as other murine bone wound models, will be informative in developing novel targets for the augmentation of abnormal inflammation following injury.

Future Directions

Future directions for this project are vast and far-reaching. As a whole, the literature that characterizes preclinical models of fracture healing, particularly in the craniofacial region, are somewhat lacking. Even sparser, is literature providing a thorough characterization of the adverse side effects associated with rhBMP-2 delivery beyond clinical observation. This is especially important considering that rhBMP-2 is used so widely, well outside the confines of its clinical indications. It is necessary to establish a variety of preclinical models that closely model the four clinical indications as well as models to address problems in rhBMP-2's off-label use.

Using a sub-critical sized defect model found in this study may allow for signaling across surgical margins to enhance the inflammatory response. If it is true that the critical sized defect does not allow for appropriate signaling, this avenue could provide a remedy. It would be interesting to investigate whether normal inflammatory signaling is affected in other non-union fracture models and in the clinical population. Obtaining human inflammasome samples as well as exploring other fracture non-union models would provide data to answer some of these

important questions. Adding a challenge to the fracture/inflammation environment, via bacterial infection for example, could also provide additional data that would allow for the proper testing of our model as it relates to the patient.

A necessary comparison that should be addressed in future research is that of an empty critical sized defect as it compares to a critical sized defect implanted with ACS. This project was aimed at identifying an alternative scaffold that could potentially be used to delivery rhBMP-2 and is clinically relevant. As such, the current clinical standard is intervention through implantation of an osteoconductive matrix. Therefore, an empty defect was not part of this clinically relevant study design. In retrospect, characterizing the completely untreated inflammatory response would allow for definitive conclusions to be made on the role that rhBMP-2 plays in modulating inflammation at this dose. This will be particularly challenging as one of the strengths of adding ACS, and osteoconductive scaffold, is that cells have a place on which to adhere throughout the center of the defect, allowing for high protein yields when doing downstream experimentation. Particularly at these early time points, the amount of biological activity in the center of the critical sized defect is likely to be very low and it is likely that the presence of scar formation would be necessary to obtain meaningful data. Despite this challenge, this is still necessary and informative experimentation.

In addition to the empty critical sized defect groups, next-step experimentation would be a clinical dose delivery of rhBMP-2 and subsequent inflammatory response characterization. Preliminary data from our group has shown that the clinical dose of rhBMP-2 parallels clinical outcomes in humans, resulting in the adverse side effect of ectopic bone formation in a murine calvarial critical sized defect. However, there has yet to be investigation into whether inflammation is up-regulated in response to scaled clinical doses of rhBMP-2 in a preclinical model. This may provide more relevant data to the current clinical state and provide the necessary foundational work to reevaluate the dosing schema that is currently used. Based on these data and that of in clinic, it is almost certain that clinical dosing of rhBMP-2 would result in heightened

inflammation. The amount of bone that is precipitated following this therapeutic and the short time in which it is deposited likely leads to further and sustained damage of the defect and surrounding tissues. Furthermore, the destruction of cells in the regenerate and surrounding tissues would signal to resident and recruited macrophages, leading to a strong M1-like pro-inflammatory response. Addressing the problems associated with rhBMP-2 delivery may simply be answered and re-evaluating the current dosing schema used in clinic.

A potential avenue for more directly evaluate macrophage polarization following administration of rhBMP-2 would be to use interrogation methods that are more stringent in their identification of an M1 vs. M2 macrophage. Indeed, it is well established that the ideas surrounding macrophage polarization *in vivo* is heavily debated. Sub-phenotypes of macrophages are readily identified *in vitro*; thus, strategies aimed at addressing how rhBMP-2 polarizes macrophages *in vitro* would be informative. This could be assessed through flow cytometry for surface markers of M1/M2 macrophages as well through *in vitro* ICC imaging. Further, the markers of macrophage polarization chosen for this experiment are widely accepted as being associated with macrophage polarization but are secreted factors that have roles in a variety of biological processes. As before, it would be informative to look at surface markers of M1/M2 polarization (i.e. Mac2 and YM1) in immunohistochemistry sections. This may more accurately distinguish distinct macrophage populations.

Using pGlcNAc as a therapeutic approach in fracture healing is still uncertain. This data has shown that pGlcNAc does not dramatically dampen inflammation in a bone wound in and of itself. Our group has shown that pGlcNAc negatively affects the amount of bone wound healing at definitive time points. In an effort to investigate this observation, our group found that pGlcNAc inhibits Smad activity critical to BMP signaling. For this reason, a combination therapy combining rhBMP-2 with pGlcNAc is unlikely to be successful in augmenting bone wound healing. However, this experimentation may provide insight into how the pGlcNAc and rhBMP-2 may result in decreased overall inflammation. Additionally, combining pGlcNAc with rhBMP-2

may result in better retention of rhBMP-2 as well as reducing the caustic side effects associated with the clinical dose of rhBMP-2. This is an area of current investigation for our group.

Final Remarks

The adverse side-effects associated with rhBMP-2 administration are vastly understudied. Furthermore, understanding how these adverse side effects can be altered through additional or subsequent therapies is not fully understood. In fact, baseline characterization of an *acellular collagen sponge* (ACS) scaffold in bone wounds is still not complete. This study aimed to tackle these questions through the use of an *in vivo* calvarial critical sized defect model. It was found that very little modulation of cellular infiltration, macrophage polarization, or angiogenesis occurred in the ACS alone group over a normal inflammatory timeline. In contrast to what was expected, delivery of a subclinical rhBMP-2 dose resulted in very little increase in pro-inflammatory markers. Macrophages were not polarized to an early M1 phenotype or a delayed M2 phenotype with ACS alone. In fact, pathological data indicated that this dose of rhBMP-2 may even potentiate an early fibroblastic healing phenotype. Thus, a slight adjustment in dose delivered to the patient may provide for optimal healing outcomes. It was also found that pGlcNAc did not significantly reduce inflammation in this model. Further, pathological data suggested that pGlcNAc may even be precipitating a longer caustic, neutrophilic response in an effort to clear the scaffold. Definitive conclusions about these therapeutics will require additional experimentation. Ultimately, extensive research is necessary to address the wide array of problems associated with bone tissue engineering and wound healing.

BIBLIOGRAPHY

1 Michalski Megan, N. M. Macrophages and skeletal health. *Pharmacology and Therapeutics* **174**, 43-54 (2017).

2 Loi, F. *et al.* Inflammation, Fracture and Bone Repair. *Bone* **86**, 119-130, doi:10.1016/j.bone.2016.02.020 (2016).

3 Ross, F. P. in *Primer on the Metabolic Bone Diseases and Disorders of Mineral Metabolism, Eighth Edition* (ed C. J. Rosen) Ch. Chapter 3, (John Wiley & Sons, Inc., 2008).

4 Myeroff Chad, C. Autogenous bone graft: donor sites and techniques. *Journal of Bone and Joint Surgery - American Volume* **93**, 2227-2236 (2011).

5 Reininger, D., Cobo-Vázquez, C., Monteserín-Matesanz, M. & López-Quiles, J. Complications in the use of the mandibular body, ramus and symphysis as donor sites in bone graft surgery. A systematic review. *Medicina Oral, Patología Oral y Cirugía Bucal* **21**, e241-e249, doi:10.4317/medoral.20938 (2016).

6 Pape Hans Christoph, H. C. Autologous bone graft: properties and techniques. *Journal of Orthopaedic Trauma* **24**, 36-40.

7 Silber Jeff, S. J. Donor site morbidity after anterior iliac crest bone harvest for single-level anterior cervical discectomy and fusion. *Spine* **28**, 134-139 (2003).

8 Snowden Cecelia, B. C. Costs of medically treated craniofacial conditions. *Public Health Reports* **118**, 10-17 (2003).

9 Amini Ami, R. A. Bone tissue engineering: recent advances and challenges. *Critical reviews in biomedical engineering* **40**, 363-408 (2012).

10 Sarkar Swapan Kumar, S. K. Hard tissue regeneration using bone substitutes: an update on innovations in materials. *Korean Journal of Internal Medicine, The* **30**, 279-293 (2015).

11 Giannoudis Peter, V. P. Bone substitutes: an update. *Injury* **36**, 20-27 (2005).

12 James Aaron, W. A. A Review of the Clinical Side Effects of Bone Morphogenetic Protein-2. *Tissue Engineering Part B: Reviews* **22**, 284-297 (2016).

13 Zara Janette, N. J. High doses of bone morphogenetic protein 2 induce structurally abnormal bone and inflammation in vivo. *Tissue Engineering Part A* **17**, 1389-1399 (2011).

14 Bastian Okan, O. Systemic inflammation and fracture healing. *Journal of Leukocyte Biology* **89**, 669-673 (2010).

15 Waters, R. V. R. Systemic corticosteroids inhibit bone healing in a rabbit ulnar osteotomy model. *Acta Orthopaedica Scandinavica* **71**, 316-321 (2000).

16 Geris Liesbet, L. Angiogenesis in bone fracture healing: a bioregulatory model. *Journal of Theoretical Biology* **251**, 137-158 (2008).

17 Hahn, E. E. *Characterization and Quantification of gene expression of rhBMP 2 Induced Inflammatory Response in Craniofacial Regeneration: A Rat Calvaria Critical Size Defect Study* Master of Science thesis, Augusta University, (2016).

18 Huang Hairong, H. The Acute Inflammatory Response to Absorbed Collagen Sponge Is Not Enhanced by BMP-2. *International Journal of Molecular Sciences* **18** (2017).

19 Buckwalter, J. A., Glimcher, M. J., Cooper, R. R., Recker, R. . Bone biology. *Journal of Bone and Joint Surgery - American* **36** (1995).
20 and, S. W. & Wagner, H. D. THE MATERIAL BONE: Structure-Mechanical Function Relations. *Annual Review of Materials Science* **28**, 271-298, doi:10.1146/annurev.matsci.28.1.271 (1998).
21 Burstein, A. H. A. Aging of bone tissue: mechanical properties. *Journal of Bone and Joint Surgery - American Volume* **58**, 82-86 (1976).
22 Marks, S. C. S. Bone cell biology: the regulation of development, structure, and function in the skeleton. *The American journal of anatomy* **183**, 1-44 (1988).
23 Parfitt, A. M., Mundy, G. R., Roodman, G. D., Hughes, D. E. & Boyce, B. F. Theoretical perspective: A new model for the regulation of bone resorption, with particular reference to the effects of bisphosphonates. *Journal of Bone and Mineral Research* **11**, 150-159, doi:10.1002/jbmr.5650110203 (1996).
24 Parfitt, A. M. What is the normal rate of bone remodeling? *Bone* **35**, 1-3, doi:https://doi.org/10.1016/j.bone.2004.03.022 (2004).
25 Fazzalari, N. L. Bone remodeling: A review of the bone microenvironment perspective for fragility fracture (osteoporosis) of the hip. *Seminars in Cell & Developmental Biology* **19**, 467-472, doi:https://doi.org/10.1016/j.semcdb.2008.08.003 (2008).
26 Parfitt, A. M. A. Misconceptions (2): turnover is always higher in cancellous than in cortical bone. *Bone* **30**, 807-809 (2002).
27 Ireton Jordan, E. J. The role of wound healing and its everyday application in plastic surgery: a practical perspective and systematic review. *Plastic and Reconstructive Surgery - Global Open* **1**.
28 Kalfas, I. H. I. Principles of bone healing. *Neurosurgical Focus* **10** (2001).
29 Costantino Peter, D. P. Bone healing and bone substitutes. *Facial Plastic Surgery* **18**, 13-26 (2002).
30 Mackie, E. J., Ahmed, Y. A., Tatarczuch, L., Chen, K. S. & Mirams, M. Endochondral ossification: how cartilage is converted into bone in the developing skeleton. *Int J Biochem Cell Biol* **40**, 46-62, doi:10.1016/j.biocel.2007.06.009 (2008).
31 Mountziaris Paschalia, M. P. Modulation of the inflammatory response for enhanced bone tissue regeneration. *Tissue Engineering Part B: Reviews* **14**, 179-186 (2008).
32 Pape Hans-Christophe, H. C. Trauma-induced inflammation and fracture healing. *Journal of Orthopaedic Trauma* **24**, 522-525 (2010).
33 Sinder Benjamin, P. B. Macrophages: Their Emerging Roles in Bone. *Journal of Bone and Mineral Research* **30**, 2140-2149 (2015).
34 Mosser David, M. D. Exploring the full spectrum of macrophage activation. *Nature Reviews Immunology* **8**, 958-969 (2008).
35 Yang Jiyeon, J. Monocyte and macrophage differentiation: circulation inflammatory monocyte as biomarker for inflammatory diseases. *Biomarker Research* **2** (2014).
36 Johnson Amy, R. A. The inflammation highway: metabolism accelerates inflammatory traffic in obesity. *Immunological Reviews* **249**, 218-238 (2012).

37 Haubruck Patrick, P. The treatment of nonunions with application of BMP-7 increases the expression pattern for angiogenic and inflammable cytokines: a matched pair analysis. *Journal of inflammation research* **9**, 155-165 (2016).
38 Bauer, T. W. T. Bone graft materials. An overview of the basic science. *Clinical orthopaedics and related research*, 10-27 (2000).
39 Molinari Robert, W. R. The Use of Bone Morphogenetic Protein in Pediatric Cervical Spine Fusion Surgery: Case Reports and Review of the Literature. *Global Spine Journal* **6**, 41-46 (2016).
40 Jusino, M. A. *Role of gas molecule signaling in bone morphogenetic protein-2 mediated bone regeneration in a critical-size rat calvarial defect model* Master of Science thesis, Georgia Regents University, (2015).
41 Lee, K. S. K. Runx2 is a common target of transforming growth factor beta1 and bone morphogenetic protein 2, and cooperation between Runx2 and Smad5 induces osteoblast-specific gene expression in the pluripotent mesenchymal precursor cell line C2C12. *Molecular and Cellular Biology* **20**, 8783-8792 (2000).
42 Boerckel Joel, D. J. Effects of protein dose and delivery system on BMP-mediated bone regeneration. *Biomaterials* **32**, 5241-5251 (2011).
43 Branch Charles, L. C. Physican-directed (off-label) use of recombinant bone morphogenic protein-2: let us do it well! *Spine Journal, The* **11**, 469-470 (2011).
44 Huang, R. L. R. Exaggerated inflammatory environment decreases BMP-2/ACS-induced ectopic bone mass in a rat model: implications for clinical use of BMP-2. *Osteoarthritis and Cartilage* **22**, 1186-1196 (2014).
45 Poon Bonnie, B. Bone morphogenetic protein-2 and bone therapy: successes and pitfalls. *The Journal of pharmacy and pharmacology* **68**, 139-147 (2016).
46 Carragee Eugene, J. E. A critical review of recombinant human bone morphogenetic protein-2 trials in spinal surgery: emerging safety concerns and lessons learned. *Spine Journal, The* **11**, 471-491 (2011).
47 Aghaloo Tara, T. A study of the role of nell-1 gene modified goat bone marrow stromal cells in promoting new bone formation. *Molecular Therapy* **15**, 1872-1880 (2007).
48 Smoljanovic Tomislav, T. Six-year outcomes of anterior lumbar interbody arthrodesis with use of interbody fusion cages and recombinant human bone morphogenetic protein-2. *Journal of Bone and Joint Surgery - American Volume* **92**, 2614-2615 (2010).
49 Bach Duc-Hiep, D. H. The Dual Role of Bone Morphogenetic Proteins in Cancer. *Molecular Therapy Oncolytics* **8**, 1-13 (2018).
50 Zabkiewicz Catherine, C. Bone morphogenetic proteins, breast cancer, and bone metastases: striking the right balance. *Endocrine-Related Cancer* **24**, 349 (2017).
51 Robin Brett, N. B. Cytokine-mediated inflammatory reaction following posterior cervical decompression and fusion associated with recombinant human bone morphogenetic protein-2: a case study. *Spine* **35**, 1350-1354 (2010).
52 Corbin Terry, P. T. Does bone morphogenetic protein increase the incidence of perioperative complications in spinal fusion? A comparison of 55,862 cases of spinal fusion with and without bone morphogenetic protein. *Spine* **37** (2012).

53 Lindner Haley Buff, H. B. Anti-bacterial effects of poly-N-acetyl-glucosamine nanofibers in cutaneous wound healing: requirement for Akt1. *PLos One* **6** (2011).
54 Lindner Haley Buff, H. B. pGlcNAc Nanofiber Treatment of Cutaneous Wounds Stimulate Increased Tensile Strength and Reduced Scarring via Activation of Akt1. *PLos One* **10** (2015).
55 Muise-Helmericks Robin, C. R. Poly-N-acetyl glucosamine fibers activate bone regeneration in a rabbit femur injury model. *Journal of Trauma-Injury Infection and Critical Care* **71**, 194-196 (2011).
56 Scherer Saja Sandra, S. S. Poly-N-acetyl glucosamine nanofibers: a new bioactive material to enhance diabetic wound healing by cell migration and angiogenesis. *Annals of Surgery* **250**, 322-330 (2009).
57 Cooper Gregory, M. G. Testing the critical size in calvarial bone defects: revisiting the concept of a critical-size defect. *Plastic and Reconstructive Surgery* **125**, 1685-1692 (2010).
58 Cui Zhong-Kai, Z. K. Design and Characterization of a Therapeutic Non-phospholipid Liposomal Nanocarrier with Osteoinductive Characteristics To Promote Bone Formation. *ACS Nano* **11**, 8055-8063 (2017).
59 Gohil Shalini, V. S. Spatially controlled rhBMP-2 mediated calvarial bone formation in a transgenic mouse model. *International Journal of Biological Macromolecules* **106**, 1159-1165 (2018).
60 Gomes, P. S. P. Rodent models in bone-related research: the relevance of calvarial defects in the assessment of bone regeneration strategies. *Laboratory Animals* **45**, 14-24 (2011).
61 Herberg Samuel, S. Mesenchymal stem cell expression of SDF-1b synergizes with BMP-2 to augment cell-mediated healing of critical-sized mouse calvarial defects. *Journal of tissue engineering and regenerative medicine* **11**, 1806-1819 (2017).
62 Li Jian, J. Visualizing Angiogenesis by Multiphoton Microscopy In Vivo in Genetically Modified 3D-PLGA/nHAp Scaffold for Calvarial Critical Bone Defect Repair. *JoVE* (2017).
63 Schmitz, J. P. J. The critical size defect as an experimental model for craniomandibulofacial nonunions. *Clinical orthopaedics and related research*, 299-308 (1986).
64 Shakir Sameer, S. Transforming growth factor beta 1 augments calvarial defect healing and promotes suture regeneration. *Tissue Engineering Part A* **21**, 939-947 (2015).
65 Kinsella Christopher, R. C. Recombinant human bone morphogenetic protein-2-induced craniosynostosis and growth restriction in the immature skeleton. *Plastic and Reconstructive Surgery* **127**, 1173-1181.
66 Kilkenny, C. C. Improving bioscience research reporting: the ARRIVE guidelines for reporting animal research. *Osteoarthritis and Cartilage* **20**, 256-260 (2012).
67 Arnold Paul, M. P. Heterotopic ossification following single-level anterior cervical discectomy and fusion: results from the prospective, multicenter, historically controlled trial comparing allograft to an optimized dose of rhBMP-2. *Journal of Neurosurgery: Spine* **25**, 292-302 (2016).

68 Boniakowski Anna, E. A. Macrophage-Mediated Inflammation in Normal and Diabetic Wound Healing. *Journal of Immunology, The* **199**, 17-24 (2017).
69 Schmidt-Bleek Katharina, K. Boon and Bane of Inflammation in Bone Tissue Regeneration and Its Link with Angiogenesis. *Tissue Engineering Part B: Reviews* **21**, 354-364.
70 Jilka Robert, L. R. The relevance of mouse models for investigating age-related bone loss in humans. *Journals of Gerontology: Series A, The* **68**, 1209-1217 (2013).
71 Langenfeld Elaine, M. E. Bone morphogenetic protein-2 stimulates angiogenesis in developing tumors. *Molecular Cancer Research* **2**, 141-149.
72 Rahimi Nader, N. Emerging roles of post-translational modifications in signal transduction and angiogenesis. *PROTEOMICS* **15**, 300-309 (2015).
73 Kowalczyk Jacek, J. Post-transcriptional modifications of VEGF-A mRNA in non-ischemic dilated cardiomyopathy. *Cellular Molecular Biology Letters* **12**, 331-347 (2007).
74 Kumar, V. B. S. V. B. Regulation of vascular endothelial growth factor by metabolic context of the cell. *Glycoconjugate Journal* **31**, 427-434 (2014).
75 Huang, R. L. R. Exaggerated inflammatory environment decreases BMP-2/ACS-induced ectopic bone mass in a rat model: implications for clinical use of BMP-2. *Osteoarthritis and Cartilage* **22**, 1186-1196.
76 Dunn Louise, L. Murine model of wound healing. *JoVE* (2013).

APPENDIX

Supplemental Figures

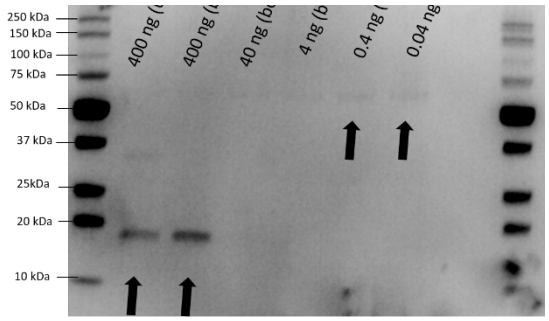

Supplemental Figure 1. *Western blot data for recombinant mouse TNF-α.* Serial dilutions of recombinant mouse cytokines revealed that the levels that were detected via cytokine array were much lower than what was detectable via western blot. Western blot analysis showed that greater than or equal to 400 ng of protein was necessary in the lysate for detection.

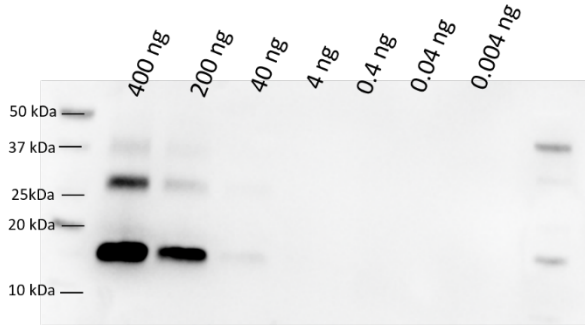

Supplemental Figure 2. *Western blot data for recombinant mouse IL-17.* Serial dilutions of recombinant mouse cytokines revealed that the levels that were detected via cytokine array were much lower than what was detectable via western blot. Western blot analysis showed that greater than or equal to 40 ng of protein was necessary in the lysate for detection.

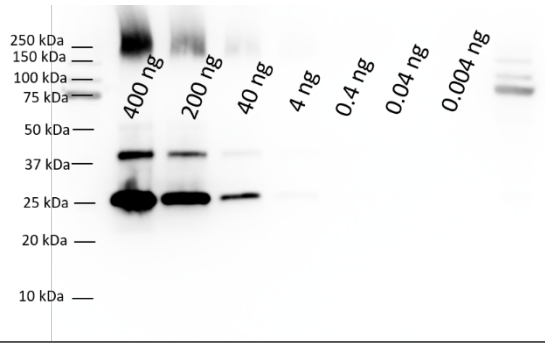

Supplemental Figure 3. *Western blot data for recombinant mouse MCP-1.* Serial dilutions of recombinant mouse cytokines revealed that the levels that were detected via cytokine array were much lower than what was detectable via western blot. Western blot analysis showed that greater than or equal to 40 ng of protein was necessary in the lysate for detection.

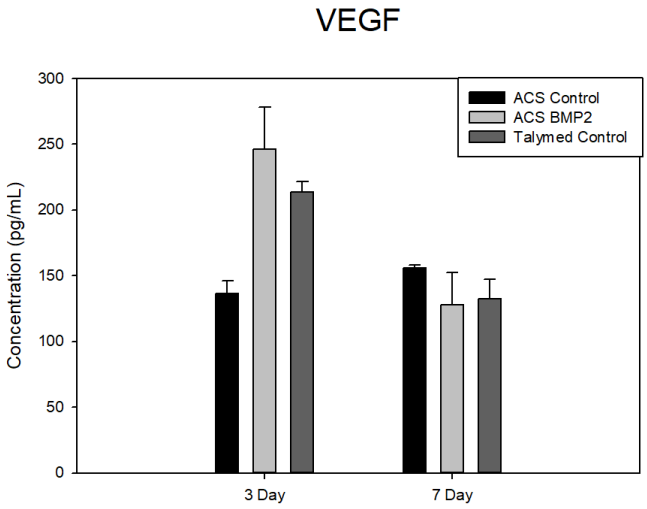

Supplemental Figures 4: *Cytokine array data for VEGF.* Cytokine array data revealed that there was a statistically significant increase in VEGF expression with the addition of rhBMP-2 or pGlcNAc at three days compared to ACS alone and a significant decrease in VEGF expression at 7 days with rhBMP-2 delivery when compared to ACS. Talymed is the trade name for the pGlcNAc nanofiber scaffold.